A Novel Methodology To Classify The ADSS Cable Ranking

by

Kumaraguru Prabakar

A Thesis Presented in Partial Fulfillment
of the Requirements for the Degree
Master of Science

Approved July 2011 by the
Graduate Supervisory Committee:

George G. Karady, Chair
Vijay Vittal
Raja Ayyanar

ARIZONA STATE UNIVERSITY

August 2011

ABSTRACT

All-dielectric self-supporting (ADSS) fiber optic cables are used for data transfer by the utilities. They are installed along high voltage transmission lines. Dry band arcing, a phenomenon which is observed in outdoor insulators, is also observed in ADSS cables. The heat developed during dry band arcing damages the ADSS cables' outer sheath. A method is presented here to rate the cable sheath using the power developed during dry band arcing.

Because of the small diameter of ADSS cables, mechanical vibration is induced in ADSS cable. In order to avoid damage, vibration dampers known as spiral vibration dampers (SVD) are used over these ADSS cables. These dampers are installed near the armor rods, where the presence of leakage current and dry band activity is more. The effect of dampers on dry band activity is investigated by conducting experiments on ADSS cable and dampers.

Observations made from the experiments suggest that the hydrophobicity of the cable and damper play a key role in stabilizing dry band arcs. Hydrophobicity of the samples have been compared. The importance of hydrophobicity of the samples is further illustrated with the help of simulation results. The results indicate that the electric field increases at the edges of water strip. The dry band arcing phenomenon could thus be correlated to the hydrophobicity of the outer surface of cable and damper.

This thesis is dedicated to my parents,

Mr. Prabakar and Mrs. Thanakumari Prabakar

ACKNOWLEDGEMENT

I wish to express my sincere gratitude to Dr. George G. Karady, for his guidance, comments, suggestions and support. I wish to thank Dr. Vijay Vittal and Dr. Raja Ayyanar for their valuable time and also for being a part of the supervisory committee. I would like to thank Dr. Sadik Kucuksari for his help on projects related to the thesis. Finally, I would like to thank my friends for their support.

TABLE OF CONTENTS

Page

CHAPTER Page

LIST OF TABLES

LIST OF FIGURES

Figure Page

Figure Page

Figure Page

NOMENCLATURE

θ	Contact angle
ε_0	Permittivity of free space
Ω/m	Ohms per meter
ADSS	All-dielectric self-supporting fiber optic cable
ASTM	American society for testing and materials
C_{aN}	Capacitance between phase A and the cable at section N
C_{gN}	Capacitance between ADSS cable and the ground at section N
C_{th}	Thévenin equivalent capacitance at section N
C	Capacitor used in the RC bank
DEIS	Dielectrics and electrical insulation society
HC	Hydrophobicity classification
I	Leakage current
IEEE	Institute of electrical and electronics engineering
I_N	Current flowing from N+1 section to section N
I_{sc}	Short circuit current
kΩ	kilo ohm
kV	Kilo volt
MΩ	Mega ohm
m	Meter
mA	milli ampere
mm	Millimeter
OPGW	Optical ground wire

PA	Polyamide
PE	Poly-ethylene
pF	Pico Farad
PT	Potential transformer
Q_k	charge due to k th line
R1	Resistor used in RC bank
R2	Resistor used to measure leakage current
RTV	Room temperature vulcanization
SVD	Spiral vibration damper
UK	United Kingdom
US	United states
$Varia_N$	Variable a at section N
$Varib_N$	Variable b at section N
V_{in}	Supply voltage
V_{ln}	line to neutral voltage
V_{oc}	Open circuit voltage
V_N	Voltage at section N
V_{sa}	Phase A voltage
V_{sN}	Equivalent voltage at node N
V_{spacek}	Space potential due to line k
WRAP	spiral WRAP fiber optic cable
x_f	x co-ordinate of ADSS cable
x_k	x co-ordinate of line k

y_f	y co-ordinate of ADSS cable
y_k	y co-ordinate of line k
Y_{xca}	capacitive admittance between phase A and ADSS cable
Y_{xcg}	Capacitive admittance between ADSS cable and ground
Y_{xN}	Thévenin equivalent admittance at section N
Y_{ra}	resistive admittance due to pollution
Y_{thev}	Thévenin equivalent admittance
W	Watt

Chapter 1

Background on ADSS fiber optic cables and dry band arcing

Telegraphy using copper conductors was the beginning of wire transmission technology which dates back 120 years. As technology improved, the way to transfer data took various forms. In 1974, fiber was made into a cable and was introduced in the field as a way to transfer data [1]. Small scale and large scale installation of these cables followed the increasing need for better communication in early 80's.

I. DIFFERENT TYPES OF FIBER OPTIC CABLES

In order to satisfy the needs of diversified fiber optic cable design and varied working environment of fiber optic cables, a number of cable construction designs were made available in the industry. These fiber optic cables can be installed along with transmission lines and could be supported at the transmission towers. This is an effective use of right of way, as the fiber cables can be used for the utility's internal data communication and excess available fibers can be leased to others. Three important types of fiber optic cables used by the utilities are

A. Optical ground wire (OPGW),

B. WRAP type fiber optic cable and

C. All-Dielectric Self-Supporting (ADSS) fiber optic cable.

A. Optical ground wire

OPGW has its optical fibers inside concentric stranded metallic wires. It has both the electrical properties and mechanical strength of a stranded metallic ground wire and also has the optical transmission properties of optical fibers.

OPGW can be installed where new ground wire is planned to be installed or by replacing the existing ground wire.

B. WRAP type fiber optic cables

WRAP type fiber optic cables are cables that are wrapped around the ground wire. When WRAP type fiber optic cables are installed, a certain amount of tension should be maintained while wrapping, in order to avoid damage to the fiber optics in the long term. WRAP type cable requires fault and lightning protection.

C. All-dielectric self-supporting fiber optic cables

ADSS cable, as the name suggests are self-supporting and are installed in a way similar to overhead transmission line conductors. But, they are installed separate from the power system, usually below the phase conductors. The mechanical strength to the ADSS cable is provided by the central strength member around which the loose buffers are stranded. The material and structure of the central strength member are selected to keep the elongation of the cable at 0.2% or less [1]. The central strength member is fabricated from fiber glass filaments bonded in resin or aramid yarn filaments [2]. Optical fibers are housed in loose buffer tubes to provide adequate mechanical protection. The tubes are filled with a gel that prevents cracks in the fibers. Solid Polyethylene (PE) buffer tubes known as fillers are stranded with the buffers [1]. Buffers are nothing but solid polyethylene tubes used to fill space and also to give additional strength to the cable. Cable sheath which is present in the ADSS cable protects the core from

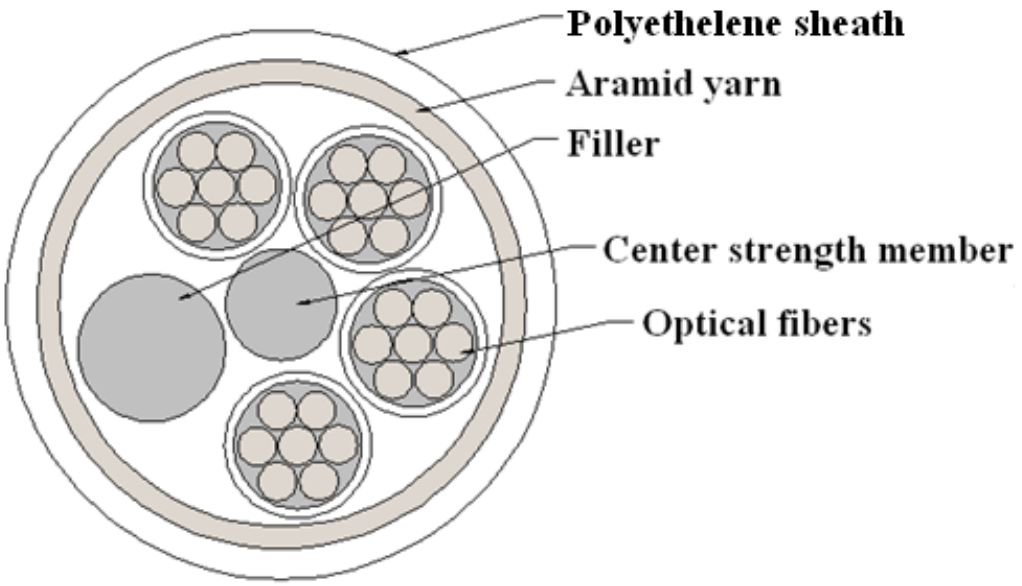

Figure. 1 Cross section of an ADSS fiber optic cable

thermal, mechanical and chemical effects. The cable sheath prevents the moisture in the atmosphere from entering the fibers present inside the cable.

An ADSS fiber optic cable is similar to a WRAP type fiber optic cable. WRAP type cables lack the central strength member that ADSS cables possess. One more advantage that ADSS cables possess over WRAP type is the increased number of fiber count which results in increased data transfer through ADSS cable. An ADSS cable could be seen as a solution when there is a need for increased number of fiber counts and also when replacing ground wire could prove to be more expensive than installing ADSS cable in the existing tower structure.

As ADSS cables are made for working with high voltage transmission lines, the outer jacket is made of special polymers to prevent the cable from damage due to electrical discharges. The cross section of a typical ADSS cable is shown in Figure. 1. Usually the outer jacket is made out of Polyethylene (PE), and

for voltage levels above 138 kV the material used is a special, track resistant polymer. PE is one of the popular materials used to manufacture the outer sheath. PVC and for some special applications Polyamide (PA) protective covers are also used to manufacture the outer sheath. In order to reduce tensile stress and pressure on ADSS cables, an additional armoring is provided to protect the optical cable core and the cable sheath.

II. DESCRIPTION OF ADSS CABLE FAILURE

ADSS cables were initially installed in transmission lines below 138 kV and they showed successful operation for a long time. Due to their successful operation, ADSS cables were installed along with transmission lines with voltage levels beyond 138 kV. Even though ADSS cables performed successfully for voltage levels below 138 kV increased number of ADSS cable failure was observed when the cables were installed in transmission lines above 138 kV [3]. Even though ADSS cables were economical and had some advantages as mentioned earlier, the failures seem to be a drawback for ADSS cable as they will cause loss of valuable data and also monetary losses will be incurred as the fiber optics are also leased to others. The cable is considered to be failed when the optical fibers are exposed due to the outer sheath failure or the cable is dropped due to strength member failure. The reasons for these failures were found through investigations on these failed cables [3] and from experimental work [4]. They are

A. Corona, and

B. Dry band arcing

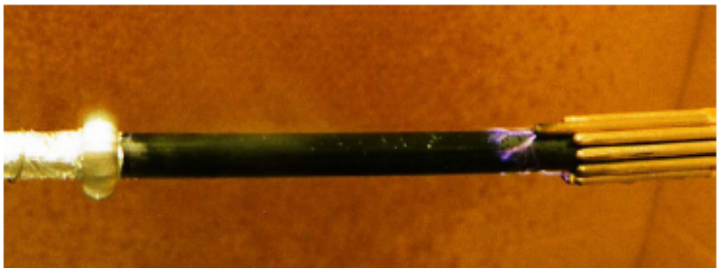

Figure. 2 Arcing near armor rod [5]

When ADSS cables are placed in the electric field created by the overhead transmission lines, the outer layer of the ADSS cable erodes due to electrical discharge. ADSS cables are installed in transmission towers with mechanical support being provided by armor rods at the tower structure. The armor rods are grounded at the transmission tower structure. There is an increased electrical discharge between the tips of the armor rod and the outer sheath of ADSS cables. The surface of the ADSS cable sheath near the armor rod suspension points undergoes a change in appearance and structure due to the increased electrical discharge near the armor rod end points. The space potential drops near the fittings and this rate of decrease cause the air around the fitting to break down and the heat developed during this discharge can cause damage to the cable surface. Corona damage can be prevented by rounding the tips, which has a distributing effect on the stress concentration and keeps the arc away from the cable sheath [4]. Figure. 2 shows arcing between the tip of armor rods and the ADSS cable [5].

OPGW do not have corona losses because they are immune from electrical field as they are placed inside the ground wires. WRAP type cables have corona discharge in the lines on which they are wrapped. Research work has been done to reduce electrical discharge near the armor rods and methods to reduce this phe-

nomenon could be found in the literature [5]. Detailed explanation about dry band arcing is presented in the upcoming section.

III. DRY BAND ARCING ON ADSS CABLES

Distributed capacitance between the ADSS cable, each phase conductor, ground wire and the ground results in a field gradient along the surface of the dielectric cable [6]. In chapter 2, this distributed capacitance is explained in detail. The surface of the ADSS cable has a high resistance (in the order of Giga ohms) usually, but pollution which settles on the surface can reduce this resistance (to the order of Mega ohms). This allows leakage current to flow along the cable. Visible arcing does not occur when the cable is well wetted or when it is dry [3].

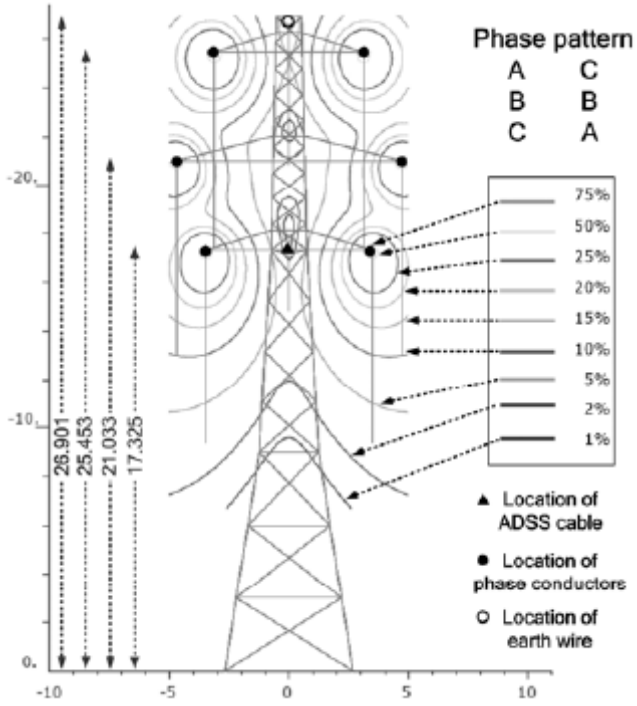

Figure. 3 Space Potential around 132 kV line, marked in percent of phase potential [6]

A wet cable suspended on a power line is likely to dry preferentially near the supports, partly because the cable slope encourages the water to drain away, and partly because the current and hence the electrical heating is highest there.

Figure. 3 shows an example of space potential in which the cables sits at the mid span. The use of space potential contours has become a standard practice to identify locations of low space potential where an ADSS cable can be installed, thereby minimizing the current to an arc [6]. The potential contour in Figure. 3 is for a 132 kV line marked in percentage of phase voltage.

IV. VIBRATION ON ADSS CABLE

When a smooth stream of air passes across a cylindrical shape, such as a conductor or an ADSS cable, eddies will be formed in the backward side of the cylindrical structure. The eddy alternate from the top and bottom surfaces and create alternating pressures that tend to produce movement at right angles to the direction of air flow [7]. The intensity of Aeolian vibration is more owing to the fact that the ADSS cable is light in weight and has a small diameter. ADSS cables are light and because of this they are prone to Aeolian vibrations. Aeolian vibration can cause severe damage to the cable and this could prove to be expensive.

In order to avoid damage, dampers are used by the utilities to dampen out the vibration. A spiral vibration damper (SVD) is an impact type damper used for damping Aeolian vibration. A spiral vibration damper reduces vibration through dissipation of vibration energy by impacting the cable. A SVD is very effective at high frequencies associated with small diameter fiber optic cables and conductors. Work has been done to prove the effectiveness of SVDs in damping Aeolian on

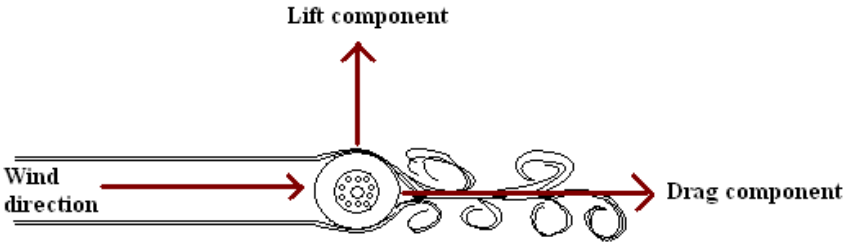

Figure. 4 Mechanism of Aeolian vibration on ADSS cable

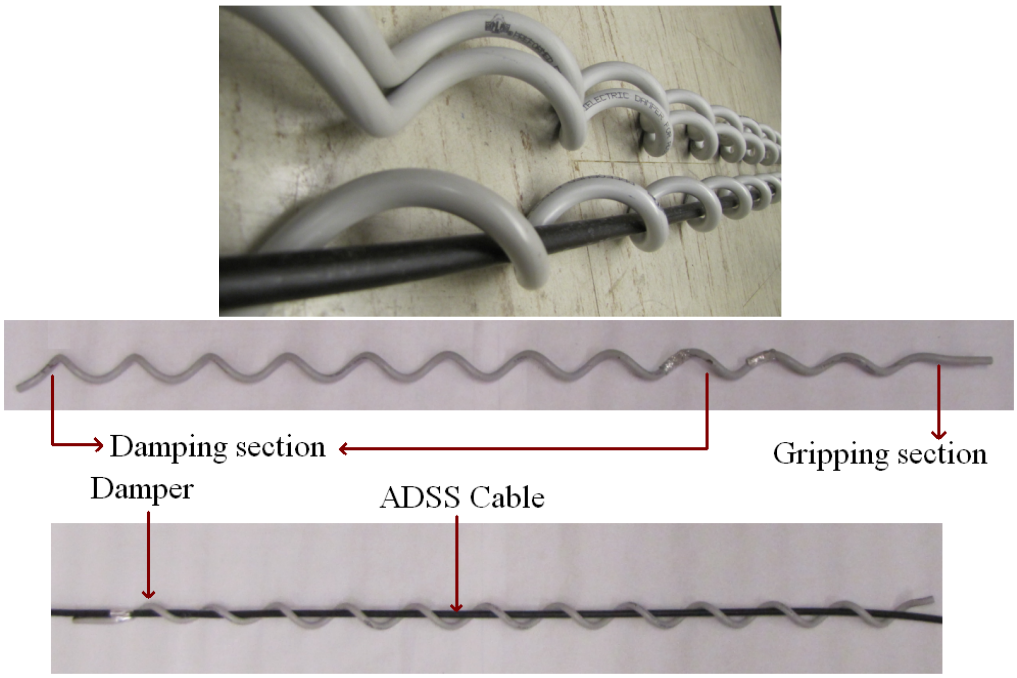

Figure. 5 Spiral vibration dampers

ADSS cables [8]. They are installed near the armor rod suspension and the numbers of dampers used between every transmission tower differ from two to four, one on either side of the tower to two on either side of tower. The number of dampers used depends on the span of the transmission line.

Spiral vibration dampers have a gripping section at one end and a damping section at the other. The radius of the helix at the damping section is larger than that at the gripping section. Figure. 6 shows the method used to install SVD's

over ADSS cables. The damper will be placed with its gripping section towards the tower structure. The damping section will be wrapped on and out from the tower structure. The installation is completed by finishing up the wrapping section. Damper could be slid out into the ADSS cable before wrapping on the gripping section. The distance between the armor rod assembly and the gripping sec-

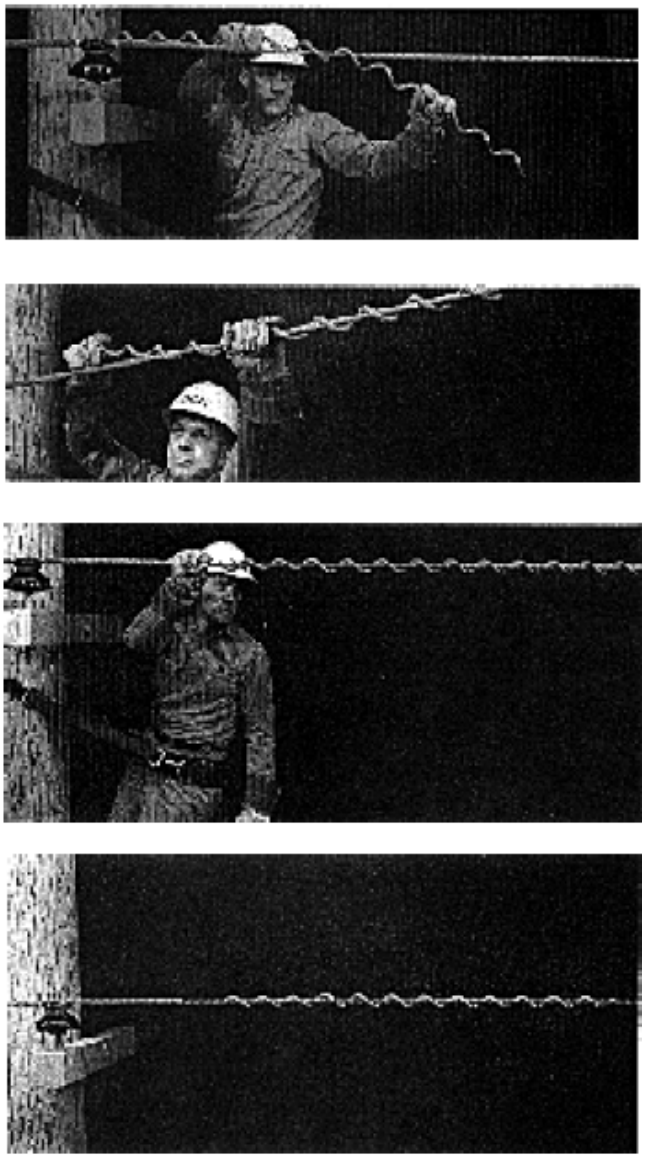

Figure. 6 Installation of spiral vibration damper [9]

tion end is around three to five inches. A similar methodology is used when installing two dampers over ADSS cables. Hot installation of the dampers is also possible by the use of a jumper holding tool.

V. ORGANIZATION OF THE THESIS

A literature survey on the research work that has been done in the past on dry band arcing in ADSS cables and the goal of this thesis is presented in chapter 2. Methods used by the utilities before installing ADSS cable and a method to calculate the power developed during the arc is presented in chapter 3. An insight on the experimental setup, sample preparation, setup of damper on ADSS cable and the results from the experiments are presented in chapter 4. Inference based on the observations made during the experiment is presented in chapter 5. In chapter 6, simulation of electric field on the surface of ADSS cable is presented and also models used for the simulation, properties of the material used and results from the simulation are shown. A conclusion based on the experiments and the simulation is presented in chapter 7.

Chapter 2

Literature review

I. INTRODUCTION

This chapter gives a review of the available literature on experimental testing and simulation work done to study dry band arcing on ADSS cables. In the first section of this paper a short introduction about the phenomenon is introduced. Then, short reviews about few papers which presented the performance of the early installation of these cables are given. This is then followed by an overview on the experimental studies available on ADSS cables. Then, an overview on the research work performed to simulate dry band arcing on ADSS cables is presented. Finally, the chapter ends with a summary of the research work done in the past and the goal of the thesis.

II. DRY BAND ARCING ON ADSS CABLE

The outer layer of ADSS fiber optic cables when it is fresh is non-conductive as it is made of dielectric material. After a certain period of time, pollution settles down on the surface of the cable and forms a semi-conductive layer in the presence of moisture. When installed along high voltage overhead transmission lines, capacitive coupling is formed between high voltage lines and ADSS cable and also between the ADSS cable and the ground. This capacitive coupling induces a voltage on the ADSS cable. This induces a current through the conductive layer. The current flow generates heat in the moist conductive layer. The wet layer will be dried due to this heat developed in small bands forming ‘dry-bands’. An arc will be formed across this dry band as an induced voltage will appear

across this dry band. The outer surface of ADSS cable will be damaged due to the heat developed due to arcing.

A. Experimental work

In [3], C. N. Carter mentions that cable failure has been observed after one year from the installation of these cables along 220 kV lines. Performance of ADSS cables was observed and the formation of dry band on ADSS cable is explained. It is mentioned in the paper that wet, polluted cables cause dry band arcing. Variation of voltage across a dry-band with position and sheath specific resistance is shown. C. N. Carter suggests that dry bands and the degradation caused by the dry band, is confined to an active length of cable adjacent to the support.

A novel design of self-supporting fiber optic cables has been proposed in [10]. U. H. P. Oestreich and H. M. Nassar calculated the voltage and current on the ADSS cable for different resistances and suggest that introduction of semi-conducting material will reduce dry band arcing phenomenon on these cables. The semi-conductive material used is a pretreated aramid yarn. The authors mention that the pretreated aramid yarn satisfies the two basic requirements, semiconduction and high mechanical strength.

In [11], cable samples from three different manufacturers were tested. The test setup had an RC circuit to simulate pollution. The test cycle included two minutes of water spraying and twenty eight minutes of drying. Current measurements were taken to check the proper operation of the test setup. Voltage applied to the setup is the maximum space potential that the cable can withstand which is 25 kV. The resistance and capacitance value of the RC circuit used is 13.1 MΩ

and 200 pF. Test results indicate the number of cycles taken by the three cable samples to fail. In order to calculate the mean time to failure rate of the three cable samples, Weibull distribution was used. Reliability curves and failure rates of the three cable samples are calculated and respective plots was shown.

When IEEE 1222 standard is used to test ADSS cables random scattering of water droplets was observed. In order to avoid the presence of random scattering of water droplets S. Kucuksari et. al in [12] proposed a new method to test ADSS cables. ASTM D2303 standard was proposed to test the cable samples. Three samples were selected and tested using the two methods. A comparison between the results has been shown and it was observed that both the methods provided similar results. But, the time taken by the cable to fail was increased in the ASTM D2303 method. In addition, ASTM D2303 did not include the current limiting RC circuit. In order to improve these parameters a new method by including the inclined plane and the RC current limiting circuit to ASTM D2303 method is proposed to test ADSS cables.

Dry band arcing near armor rod tips was experimentally studied in [13]. Mechanical support to ADSS cable is provided by armor rods at the tower structure. J.D. Shikoski and G. Karady in [13] conducted electric field calculation near the armor rods. The authors varied the length of termination of the armor rods and obtained the electrical field distribution. Experimental testing was conducted on ADSS cable samples for different values of current limiting resistance and capacitance. The voltage and current values of the arc developed were monitored. In the experimental setup, the armor rod assembly was simulated by using brass rod ar-

rangement. High voltage was applied across the brass rods and another electrode, which was grounded. The dry band voltage and current needed for the arcing and the time when the dry band arcing begun and also the ending time were recorded for different current limiting resistance and capacitance. The dry band starting voltage, starting current, ending voltage and ending current were shown. The effect of variation of current limiting resistance and capacitance on dry band voltage, arc current, time duration of the arc, starting time and ending time of the arc were presented. Statistical data of the above mentioned parameters for different current limiting resistances and capacitances were experimentally found.

In [14], several mitigation devices to control dry band arcing in ADSS cables is proposed. C. N. Carter suggests methods that could make the arcs less stable. From theoretical and experimental work the potential available for dry band arcing is observed to be from 15 to 30 kV. It was put forward that there is a threshold value of earth leakage current below which damaging arcs will not occur. A typical value of this threshold is believed to be 0.5 mA. Data has been collected from two ADSS cable installations in UK which show that leakage current exceeds 5 mA during very bad weather conditions. Methods proposed in [14] to mitigate dry band arcing in ADSS cable are use of hydrophobic materials to reduce leakage currents, spark gaps, confining arcs to an arc resistant plaque, use of rain shield and altering the electrical coupling at the fittings. The use of any mitigation method from the above, if proven to be effective can significantly extend the cables life.

Experimental results reported in [15] suggest that when an arc is compressed the severity of the arc can be increased, which leads to cable failure considerably earlier than expected from the dry band arc model. Arc compression here indicates the reduction in length of the arc due to movement of water droplets towards each other. S. M. Rowland and F. Easthope in [15], talk about the effects of using a salt fog and also about the effects of using continuous spray. The experiments were carried out in samples which were kept horizontal and samples which were inclined by a slope. The importance of the source impedance in the failure of the cable has also been shown by varying the source impedance in the experiments. The cable samples with higher source impedances tend to fail earlier than the ones with lower source impedance. From the visual observations made during the experiments, the authors explain the behavior followed by the arc and a phenomenon called arc compression is introduced. Authors suggest that the arc will be compressed in length, when there is movement of water droplets on the surface of the cable. The sample tested in the laboratory failed earlier when there is an arc compression when compared with samples which failed due to continual erosion by stable dry band arcs.

A new test method that represents quasi-environmental conditions experienced by fiber-optic cables strung along high-voltage transmission line is introduced in [16]. The study of the effect of current limiting impedances representing heavy and light pollution levels was also presented. The effect of open circuit voltage and short circuit current on failure of the cable was introduced. The test setup used for testing ADSS cables was explained. Five test samples were simul-

taneously tested in this setup. Aluminum foils are used as electrodes and the ends of the samples are sealed to avoid moisture ingress. The cables are tested for heavy and light pollution levels with resistances of 5 MΩ and 43 MΩ and capacitances of 600 pF and 66.7 pF respectively. Short circuit current is measured by varying the applied voltage levels. The cycles needed by cables to fail were recorded. A test cycle is considered to have two minutes of water spraying and thirteen minutes of drying. The area and depth of damage were observed from the samples. It was found that the area of damage in the cable is inversely proportional to the number of cycles taken by the samples to fail. If the cables fail very fast, dry band arcing would happen over a large area instead of focusing to one certain place. The average area damage and the average depth damage for the cable samples were presented.

An alternative solution for dry band arcing was presented in [17], which has had extensive trials. The solution is based on a rod of controlled resistance

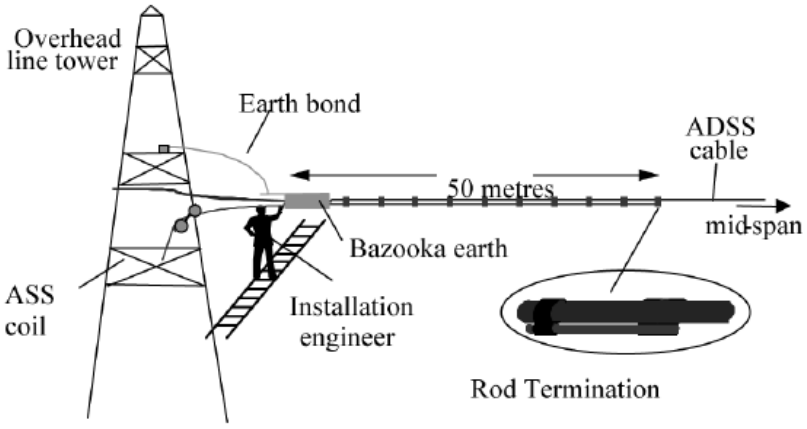

Figure. 7 Schematic of the rod installation [17]

known as the arc arrest system. This has been deployed at Chile, where sheath damage has occurred six months after the ADSS cable was originally installed. The cables have a polyethylene sheath and were supplied by a number of multinational manufacturers with a similar design, all employing aramid yarn as strength member. In majority of the cases, the sheath damage was due to relatively severe dry-band arcing near the towers. Damages have caused the aramid yarn to break and the tubes containing the optical fibers have been exposed. The damage on the cable has been graded according to the radial depth of the puncture in cable sheath. At their closest, the lines are 600 m from the ocean, and are mostly 1 to 2 km from the coast for long stretches and, here remedial work was required immediately. The resistivity of the contaminants on the ADSS cable at such locations was crudely measured to be approximately 500 kΩ/m. Potential between 7kV and 11 kV were predicted to be available on the cable layer. The ADSS cables were not installed in the optimum position to reduce induced currents. The rod prevents high fields from being built up over the ADSS cable region on which it sits, thus preventing dry band arcs occurring in that region of cable closest to the tower and also the current diminishes away from the tower. Trials have been made, currents were monitored on the system and compared to those predicted by a software model. In this case, only a very high resistance rod would be able to prevent current at its tip from being too high. The arc arrest system did not show any new damage. Even though few of the rods showed no new damage, it was not completely effective. Past installation experience showed that the sheath of the rod

ages. This is also created dry band arcing. The authors suggest that the arc arrest system was on the borderline of acceptability for high reliability.

B. Simulation work on dry band arcing

In [18], a software package named CDEGS is used to model the electrical environment of an ADSS cable. The ADSS cable under test had been taken out of service after 15 years and was installed along 132 kV transmission lines of span 314 meters. The voltage gradient and the leakage current along the surface of the ADSS cable were investigated. Relationship between modeled environment and the hydrophobicity of the cable sheath affected by this environment was analyzed. Prediction of leakage current magnitude was correlated with reductions in contact angle within a span. Due to the different clamping technologies used at tension towers and at suspension towers and also due to the differential sag between ADSS cable and the conductors, there is a change in the position of an ADSS cable relative to the phase conductors in between the two towers' span. The induced voltage on the ADSS cable at the tension tower end, suspension tower end and at the mid span was calculated and is found out to be 0.23 kV, 3.94 kV and 0.22 kV. Current magnitude was also calculated. Asymmetry in current magnitudes with respect to mid span could be observed from the results. Varying the relative position of the ADSS cable was responsible for this asymmetrical nature of the leakage current. Contact angle measurement, a measure used to identify the hydrophobicity of a material surface was calculated for the cable samples. Three cable samples were used and they are cable from service, UV aged cable and salt fog

aged cable. The contact angle measurements are correlated with the leakage current and an inverse relationship between the two was identified.

A numerical algorithm to analyze the equivalent circuit formed due to the capacitive coupling and to predict dry band arcing in fiber optic cables was presented in [19]. The sag for ADSS cable and the conductors are calculated considering a line sag of 2 % and a fiber optic cable sag of 0.2%. The entire span is divided into many sections. The capacitive coupling and the resistive pollution layer is considered to be distributed along this span. Maxwell potential coefficient was used to calculate the capacitance values. A Thévenin equivalent circuit was used to replace the three phase voltages and capacitances to simplify the calculation. Nodal equations were used to write a generalized formulation to calculate the voltage and current in each section. Heavy, medium and light pollution levels are considered with resistance values of 10^5 ohms/meter, 10^6 ohms/meter and 10^7 ohms/meter respectively. ABC and ACB phase sequences were considered in the calculation method. The authors mention that an open circuit voltage above 7 kV and low currents in the range of 0.5 mA to 1 mA is needed for steady arcing and to produce most damage. The authors also suggest that the results from this algorithm could be compared with these known values and thus a prediction of dry band arcing could be made from the comparison.

In [20], the electric field distribution along the cable surface is found using a commercially available software package known as COULOMB. Electric field distribution along the cable is responsible for initializing the arc. The simulation results are used to compare the electric field distribution on the samples by vary-

ing the thickness of the water film, shape of the water film and length of the dry band. The criteria for the arc to extend along the electrolyte surface are discussed. From the results, it was shown that the breakdown of the dry band must occur first at the edge, and then extend to the whole dry band. Initialization of dry band arcing is due to surface flash over. The thinner the water layer on the cable surface, the higher the electric field along the dry band. It is concluded that arcing is established through the cascaded breakdown of dry band and drying of the water layer by the arcs could be a dominant factor to force the arc to extend along the cable.

S. M. Rowland et. al in [21] suggest that aging of ADSS cable occur in two phases. First, a hydrophobic sheath gradually becomes hydrophilic over several years of low-current surface discharges and UV radiation. Second, dry-band arcing occurs occasionally throughout the cables' remaining life, gradually degrading its surface through tracking or erosion. A commercial package known as CDEGS is used and in particular the sub package HIFREQ is used to calculate current distributions for networks of overhead conductors and metallic grids. From the current distributions, electric field and scalar potentials at in-air and in-soil field observation points are calculated. The result obtained from the model is compared with the results shown in literature published by others. Calculations for three different values of differential sag were provided. The results are similar to the models provided by others. The effect of the presence of the tower on the current and field calculation is obtained from the model. The presence of the tower only affects the current at a distance up to 5 to 6 m from the tower. The effect is significantly more pronounced with a reduction in peak current at the tow-

ers of approximately 30%. Voltage gradients are not affected by the tower in either case. The voltage gradient is considerably reduced for the more conductive cable compared to the very resistive case. The space potential varies from less than 10% to a value slightly greater than 20%. It has been shown that at higher and more realistic cable resistivity, the tower can make a significant difference to the current to ground. This is primarily because the distance over which current is gathered is small in the high resistance case and also the length affected by the tower capacitance is of more importance. The model shown in [21] is consistent with published models of other researchers.

III. SUMMARY OF LITERATURE REVIEW

A summary of the literature review and past research work is presented below

- Models to predict the current and voltage distribution on the ADSS cable layer has been proposed.
- Prediction of dry band arcing based on current and voltage distribution on models has been proposed.
- Implementation of ASTM 2303 – Inclined plane test which is used to test insulators has been suggested to test ADSS cables.
- Aging of cable sheath has been related to the leakage current flow on the surface of ADSS cable.
- Methods like using an insulator to support the armor rods at towers and wrap the surface of ADSS cable near the armor rods with semi-conducting tape has been proposed to mitigate dry band arcing.

Figure. 8 shows capacitive coupling formed between the transmission line and the ADSS cable as explained in the literature. The resistance between each capacitive coupling is indicated by the resistor and this corresponds to the pollution on the outer layer of the cable sheath. ADSS cables are rated by the maximum space potential that the outer sheath can withstand without damage. Reference [22] suggests that it is not the efficient way to rate a cable on the space potential. It will be serving without considering the pollution in the environment, voltage and current distribution. The cable should be rated according to the voltage and current that the cable can withstand. But, this does not take into account the heat developed during the development of the arc. A more appropriate prediction of the effect of dry band arcing would be to identify the power developed

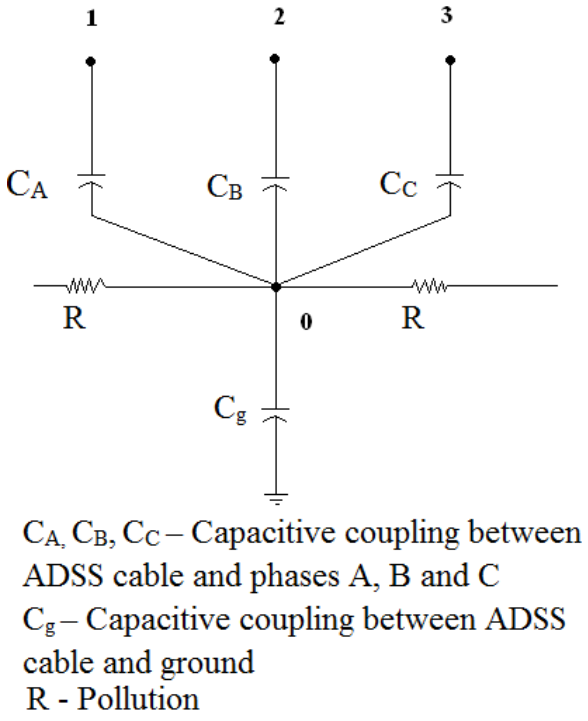

Figure. 8 Capacitive coupling between overhead lines and ADSS cable

during the arcing period and rate the cables according to the power needed to damage the cable. Table. 1 shows some of the ADSS cable failures that are reported throughout the world.

Table. 1 Reported ADSS cable failure [22]

Location	Voltage level (kV)
Cairns, Australia	132
Cape Town, South Africa	132
Gaza Strip	132
Dungeness, UK	132
Fawley, UK	132
Gaza Strip	161
Dungeness, UK	275
Fawley, UK	275
Hunterson, Scotland	400
Southern Florida, US	500

IV. AIM OF PRESENT WORK

In this thesis, a method to calculate the power generated during the development of an arc is calculated from experiments and from the results obtained, an approach to rate the cable has been proposed. The dielectric fittings and spiral vibration dampers are installed near the armor rods where the presence of electrical discharge and leakage current is more. Cable sheath damage at the dielectric fittings has been reported. An investigation of this phenomenon is conducted in this report and a conclusion based on the results from the experiments is presented.

Chapter 3

Available methods to rate ADSS cable

I. INTRODUCTION

Typical methods followed by the utilities when installing ADSS fiber optic cables in the transmission towers are explained in this chapter. The procedure for calculating space potential around the transmission line, voltage distribution and current distribution on ADSS cable are shown. A method to classify the ranking of ADSS fiber optic cables using the power developed to damage the cable surface is proposed.

II. SPACE POTENTIAL AROUND THE TOWERS

Before a utility installs ADSS cable in its transmission grid, space potential calculations around the mid span would be performed. This is advised by the cable manufacturer to identify potential problems. Most of the cable manufacturers rate their cables according to this space potential. A typical space potential contour around the mid span is given in Figure. 9. The cable manufacturer prescribes a certain maximum space potential limit at which the cable could operate without failure. The cable should be installed at the tower structure where the available space potential does not exceed the space potential limit prescribed by the manufacturer. According to Institute of Electrical and Electronics Engineers (IEEE) 1222 standard, an ADSS cable with a PE sheath can be used at positions where the space potential is not more than 12 kV and cables with anti-tracking sheath could be used at positions where the potential is anywhere between 12 kV to 25 kV [28]. The manufacturer of the cable samples used in the experiments has

cables available in the above mentioned range. The ADSS cable used in the experiments are rated for 25 kV. Cables with a rating of 12 kV is also available for installation from the manufacturer. In the tower structure shown in Figure. 9, at certain places the space potential goes below 25 kV. If a cable which is rated for a space potential of around 25 kV is installed at these places below 25 kV, dry band arcing on ADSS cable is minimum. But, if the cable is installed around places where the space potential is above 25 kV, then the outer dielectric cable sheath can be damaged due to increased dry band arcing activity. Variation in the phasing and the sag of conductors and ADSS cables can heavily influence the space potential. To have a better understanding of the above mentioned effects, the space potential around the transmission line for most of the possible phasing and space potential around the mid span of the transmission line are performed. Space potential calculation around a typical transmission line is presented in the upcoming section.

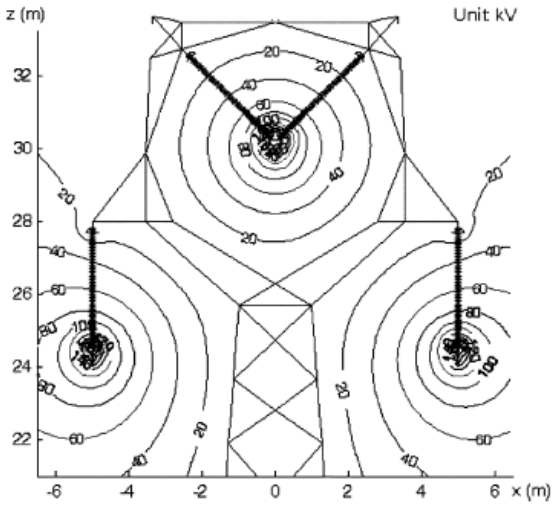

Figure. 9 Space potential around a transmission line mid span [1]

Line	Line x-position m	Line y-position m	Number of lines per bundle	Line diameter mm	Spacing in bundle mm	Line to grid voltage kV	Phase angle degrees
0	0	38.95	1	12.6	400	0	0
1	-5.3	17.25	1	27	400	127.02	0
2	-4.95	23.85	1	27	400	127.02	120
3	-4.95	30.45	1	27	400	127.02	240
4	5.3	17.25	1	27	400	127.02	0
5	4.95	23.85	1	27	400	127.02	120
6	4.95	30.45	1	27	400	127.02	240

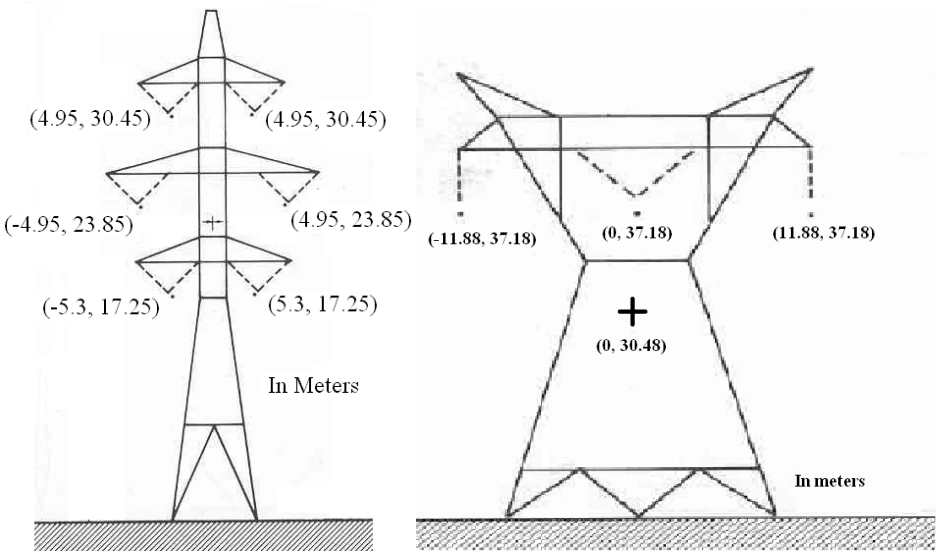

(a) (b)

Figure. 10 Models showing ADSS cable and Phase conductor position

(Model I-(a) and Model II-(b))

Table. 2 show the co-ordinates of a six phase transmission line and a probable ADSS cable location is (0 m, 21.65m). The following calculation is performed to find the space potential at the location of the ADSS cable.

Space potential due to lines 0 to 3 is

$$Vspace_k = \frac{Q_k}{2*\pi*\varepsilon_0} * \ln\left(\frac{\sqrt{(x_k - x_f)^2 + (y_k - y_f)^2}}{\sqrt{(x_k - x_f)^2 + (y_k - 0)^2}}\right) \quad (1)$$

Space potential due to lines 4 to 6 is

$$Vspace_k = \frac{Q_k}{2*\pi*\varepsilon_0} * \ln\left(\frac{\sqrt{(x_k - x_f)^2 + (y_k - y_f)^2}}{\sqrt{(x_k - x_f)^2 + (y_k - 0)^2}}\right) \quad (2)$$

Where

k = 1,2,…..,6

V_{spacek} = Space potential due to line k

x_k , y_k = x and y co-ordinates of lines 1,2,…..,6

x_f, y_f = x and y co-ordinate of the ADSS cable

Q_k = Charge due to k th line

ε_0 = Permittivity of free space

Magnitude of the space potential on the surface of the ADSS cable is

$$Vspace = \sum_k Vspace_k \tag{3}$$

= 15.373 + j.16.882 kV

$$|Vspace| = 22.8 \text{ kV} \tag{4}$$

The above mentioned method could be used to make a contour plot of the space potential around transmission lines and such a plot is shown in Figure. 9.

III. VOLTAGE AND CURRENT DISTRIBUTION ON THE SURFACE OF THE ADSS CABLE

A distributed capacitive coupling exists along the span between the phase conductors to the ADSS cable and ADSS cable to the ground [3]. Pollution that settles on the surface of the ADSS cable forms a distributed resistance along the entire span. Figure. 11 show two section of a three phase double circuit line with resistance in series between them. The admittance *Yra* represents the resistance of the pollution layer. Yxc_a, Yxc_b and Yxc_c represent the capacitive admittance formed between phase and ADSS cable, phase B and conductor cable, phase C and conductor cable. Yxc_g represent the capacitive admittance between ADSS cable and

ground. The phase conductors could be replaced by voltage sources whose values are given by (4).

$$Vs_a = V_{\ln}.1, \quad Vs_b = V_{\ln}.a^2, \; Vs_c = V_{\ln}.a$$
$$Vs_{a1} = V_{\ln}.1, Vs_{b1} = V_{\ln}.a^2, Vs_{c1} = V_{\ln}.a \qquad (5)$$

V_{ln} = Line to neutral voltage

$a = 1 \angle 120°$

Figure. 12 shows the equivalent of Figure. 11 when the phases are replaced with voltage sources. In order to simplify the circuit, the Thévenin equivalent for Figure. 12 is calculated and is shown in Figure. 13. The six voltage sources are replaced with their Thévenin equivalent V_{sN}. The capacitive coupling between phase conductors and the ADSS cable and from the ADSS cable to the ground is replaced with a Thévenin equivalent admittance Yx_N. The Thévenin equivalent voltage source and Thévenin equivalent admittance are shown in (5) and (6) respectively. In Figure. 12, the admittance *Yra* due to the pollution is not shown, but it exists between every unit section (Figure. 13).

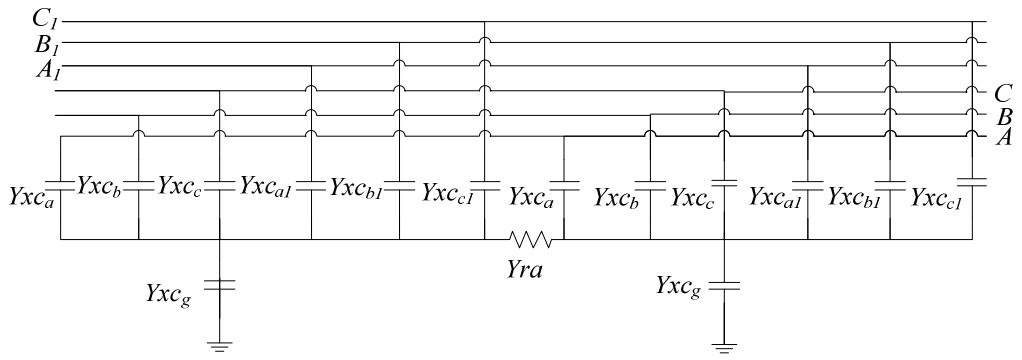

Figure. 11 Circuit showing two equivalent sections

$$Vs_N = \frac{V_{ln}\left[Yxc_{aN} + a^2 Yxc_{bN} + aYxc_{cN} + Yxc_{aN} + a^2 Yxc_{bN} + aYxc_{cN} \right]}{Yx_N} \quad (6)$$

Where

$$Yx_N = j.\omega.C_{TH_N} \quad (7)$$

$$C_{TH_N} = C_{a_N} + C_{b_N} + C_{c_N} + C_{a1_N} + C_{b1_N} + C_{c1_N} + C_{g_N} \quad (8)$$

Yxc_{aN}, Yxc_{bN}, Yxc_{cN} = Capacitive admittance formed between phase and ADSS cable, phase B and ADSS cable, phase C and ADSS cable at section N

C_{xN} = Capacitance between phase x and cable at section N

C_{gN} = Capacitance between ground and cable at section N

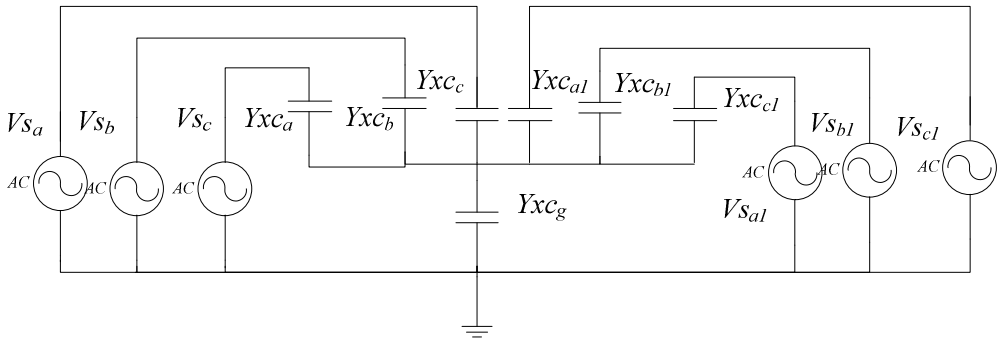

Figure. 12 Equivalent circuit with voltage sources from (6)

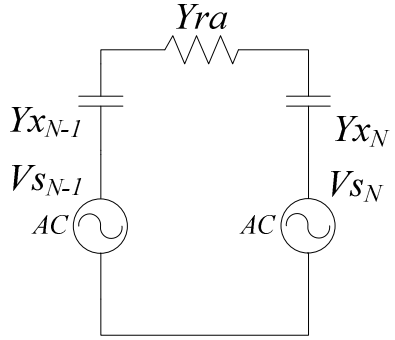

Figure. 13 Thévenin equivalent circuit

The equivalent circuit considered is grounded near the towers (Figure. 14). In Figure. 14, the entire length of the span is divided into N sections to provide a better understanding of the nodal equations used. In Figure. 14, the entire span is divided into five sections. The equivalent circuit shown in Figure. 14 is considered to be distributed along the span. The admittance value of each section will be the same if sag is not considered for calculating the value of capacitance. For the calculations presented here, sag is taken into account and each segment has a different admittance value.

A. Equations for voltage distribution

A generalized equation could be obtained from the nodal equations for the circuit shown in Figure. 14. Equations (8), (9) and (10) represents the nodal equation at node one, two and three respectively.

$$-V_0 . Yra + (Vs_0 - V_0).Yx_0 + (V_1 - V_0).Yra = 0 \quad (9)$$

$$(V_0 - V_1).Yra + (Vs_1 - V_1).Yx_1 + (V_2 - V_1).Yra = 0 \quad (10)$$

$$(V_1 - V_2).Yra + (Vs_1 - V_1).Yx_1 + (V_2 - V_1).Yra = 0 \quad (11)$$

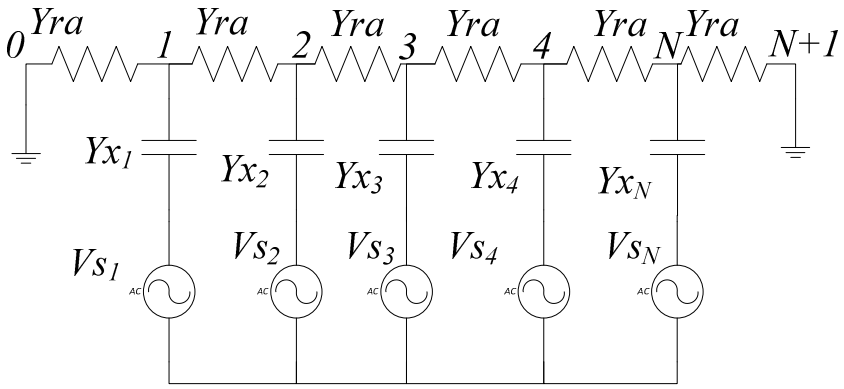

Figure. 14 Equivalent circuit for the entire length of the line

Where

Yra = Admittance due to the section resistance

V_N = Voltage at node N

By rearranging (9), (10) and (11), a generalized equation can be obtained. Equation (12) is a generalized equation for calculating the voltage at every node. The current flowing in every section for Figure. 14 can be calculated from (15). By using (12) and (15) voltage and current distribution characteristics can be calculated.

$$V_N = \begin{cases} Varia_N & If\ N = N_{sec} \\ Varia_N + V_{N+1}.Varib_N & Otherwise \end{cases} \tag{12}$$

Where

$$Varib_N = \begin{cases} \dfrac{Yra}{Yx_N + 2.Yra} & If\ N = 1 \\ \dfrac{\dfrac{Yra}{Yx_N + 2.Yra}}{1 - Varib_{N-1} \cdot \dfrac{Yra}{Yx_N + 2.Yra}} & Otherwise \end{cases} \tag{13}$$

$$Varia_N = \begin{cases} Vs_N \cdot \dfrac{Yx_N}{Yx_N + 2 \cdot Yra} & If\ N = 1 \\ \dfrac{Vs_N \cdot \dfrac{Yx_N}{Yx_N + 2 \cdot Yra} + Varia_{N-1} \cdot \dfrac{Yra}{Yx_N + 2 \cdot Yra}}{1 - Varib_{N-1} \cdot \dfrac{Yra}{Yx_N + 2 \cdot Yra}} & Otherwise \end{cases} \tag{14}$$

V_N = Voltage at node N

$$I_N = (V_{N+1} - V_N).Yra \tag{15}$$

IV. OPEN CIRCUIT VOLTAGE AND SHORT CIRCUIT CURRENT

From the Thévenin equivalent admittance of the entire span shown in Figure. 14 and from the short circuit current, the open circuit voltage can be calculated using (16).

$$V_{OC} = \frac{I_{SC}}{Y_{Thev}} \tag{16}$$

Where

$$I_{SC} = I_0 \tag{17}$$

Y_{th} = Thevenin equivalent admittance

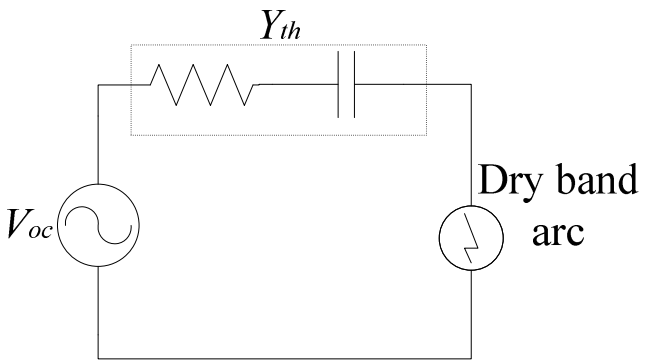

Figure. 15 Thévenin equivalent of the span

Using the above voltage and current values, the power available in the system for the dry band arc could be calculated. Equation (18) is used to calculate the power available in the system.

$$\textit{Power available in the system} = \text{Real}(V_{OC} \cdot I_{SC}) \tag{18}$$

V. MODELS AND PARAMETERS CONSIDERED FOR CALCULATION

B. Models

The voltage and current distribution on the surface of ADSS cable for a three phase double circuit line and a three phase single circuit line is shown in this section. The tower geometry for the two models used for the calculation is given in Table. 2 and Table. 3. Figure. 10 shows the tower geometry of the models used and the ADSS cable is considered to be at the position marked by a plus symbol.

Table. 3 Tower geometry for double circuit line used in voltage and current distribution calculations (model I)

ADSS cable (m)	***Phase conductors(m)***					
(X_0,Y_0)	(X_1,Y_1)	(X_2,Y_2)	(X_3,Y_3)	(X_4,Y_4)	(X_5,Y_5)	(X_6,Y_6)
(0,21.65)	(-5.3, 17.25)	(-4.95, 23.85)	(-4.95, 30.45)	(5.3, 17.25)	(4.95, 23.85)	(4.95, 30.45)

Table. 4 Tower geometry for single circuit line used in voltage and current distribution calculations (model II)

ADSS cable (m)		***Phase conductors(m)***					
X_0	Y_0	X_1	Y_1	X_2	Y_2	X_3	Y_3
0	30.48	-11.88	37.18	0	37.18	11.88	37.18

A. Effect of sag

The height of the conductor is assumed to be a hyperbolic cosine function along the span [4]. The sag of phase conductors is generally greater than the sag of the fiber-optic cable. In order to calculate the voltage and current distribution, sag of 2% for the phase conductors and sag of 0.2% for the ADSS cables were

considered .In model II, towards the middle of span, the distance between the phase conductors and the ADSS cable is reduced. The sag details of model II could be observed from Figure. 16. This will affect the capacitive coupling between the phase conductors and ADSS cable.

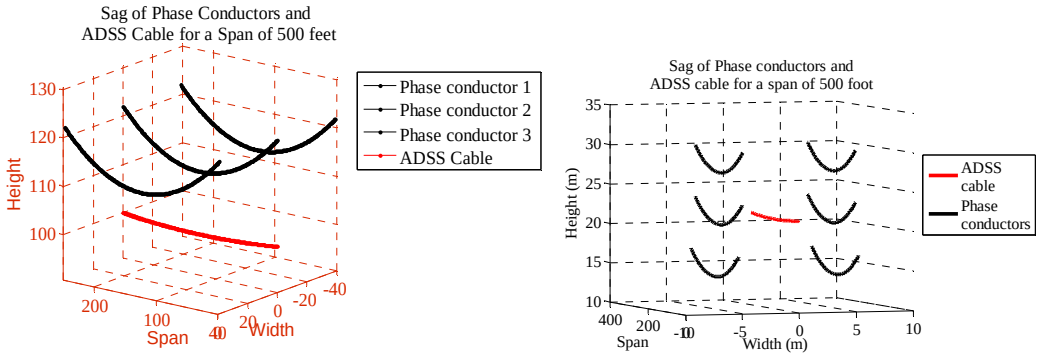

Figure. 16 Models showing ADSS cable and Phase conductor sag

B. Effect of pollution

The outer sheath of the ADSS cable is not conductive when they are installed. The outer layer of the cable is made up of dielectric materials and their resistances are in the order of 10^{12} Ω/m. Depending on the pollution of environment surrounding the cable, a conductive layer is formed on the cable. Increased pollution can increase the severity of dry band arcing, which eventually leads to

Table. 5 Resistance values for different levels of pollution

Pollution level	*Layer resistance Ω/m*
Low	10^7
Medium	10^6
Heavy	10^5

the failure of ADSS cables earlier than expected. Pollution is considered to be one of the prime factors that causes dry band arcing. Pollution typically includes salt content settled on the surface of the cable. Typical pollution resistances used for calculations are given in Table. 4

C. Voltage and current distribution

The voltage distribution for models I and II is shown in Figure. 17 and Figure. 18 respectively. Both the models were considered to have their line to neutral voltage of 220 kV. In spite of the fact that both models are considered to be working at the same voltage level, the distribution is different for both the models. The tower geometry plays a key role in the distribution of voltage. The voltage distribution is symmetric with respect to the middle of the span. The voltage level increases from a low value near the towers to a maximum near the middle span. The voltage distribution is observed to be at maximum for light and medium pollution levels and reaches a minimum for low pollution level. For model I, maximum voltage is observed near the tower for low and medium pollution. The maximum voltage for model II is observed at the middle span. It is observed from previous experience and through experiments that voltage levels greater than 10 kV are required to produce sustained arcing [5]. From Figure. 17 and Figure. 18, it is clear that there is high probability for dry band arcing, as the voltage and current distribution are higher than needed to initiate dry band arcing [5].

The current distribution for models I and II are shown in Figure. 19 and Figure. 20 respectively. The current distributions indicate that maximum current is observed near the towers. Even though the available voltage is sufficient to

strike an arc across a dry band, there is a need for sufficient amount of current flow to maintain the arc. The pattern of current distribution on the layer of the ADSS cable suggests that among the three pollution levels, the least amount of current was observed for light pollution level. The probability of arcing at low pollution levels is less due to the lack of available current to sustain the arc. As the pollution level increases the conductivity of the outer layer increases. Due to the increased conductivity, the current flow increases as the pollution level increases and reaches maximum for heavy pollution. The current flow is symmetric along the mid span. To sustain a dry band arc, current flow of 0.5 mA and higher is needed [5]. The risk of dry band arcing is near the towers rather than at the mid span because of the increased leakage current flow near the tower. Using the calculation method explained earlier, the open circuit voltage and short circuit current for three pollution levels are calculated and is shown in Table. 5.

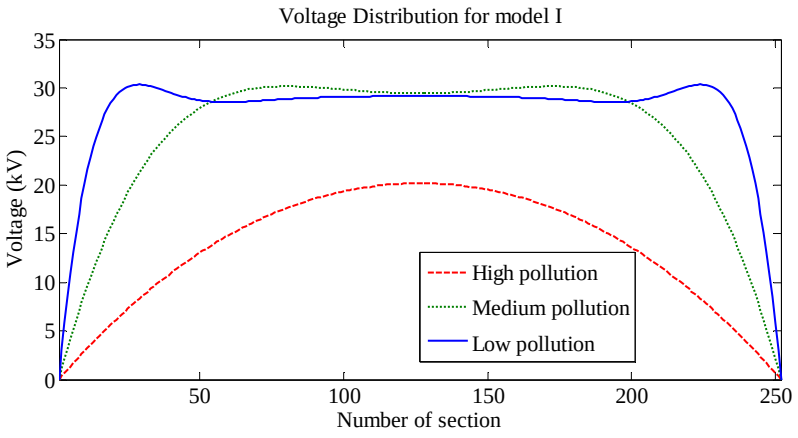

Figure. 17 Voltage distribution for model I

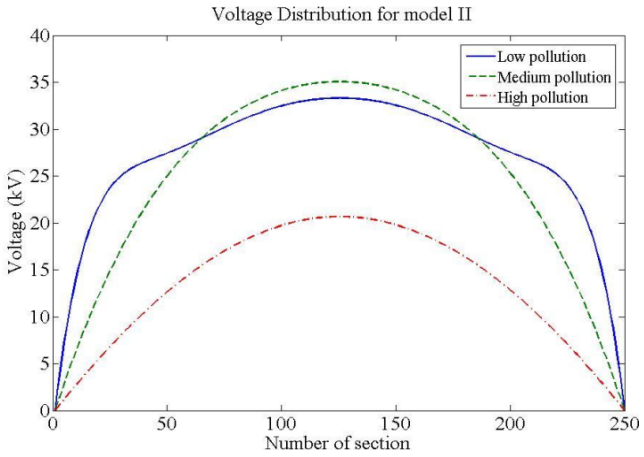

Figure. 18 Voltage distribution for model II

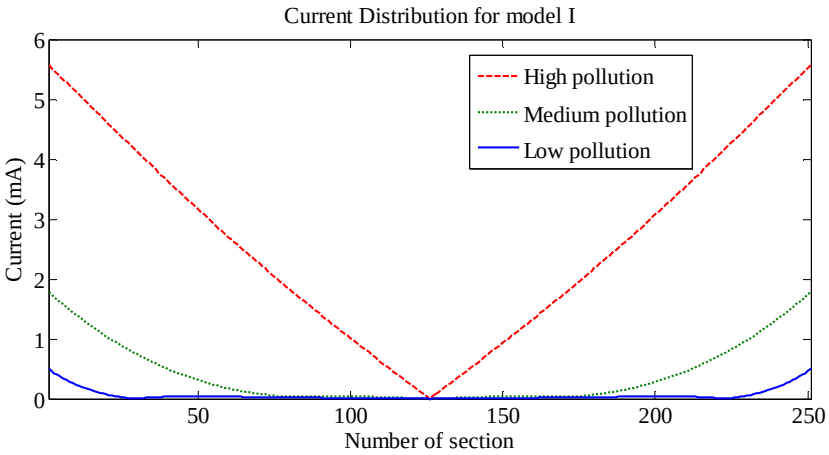

Figure. 19 Current distribution for model I

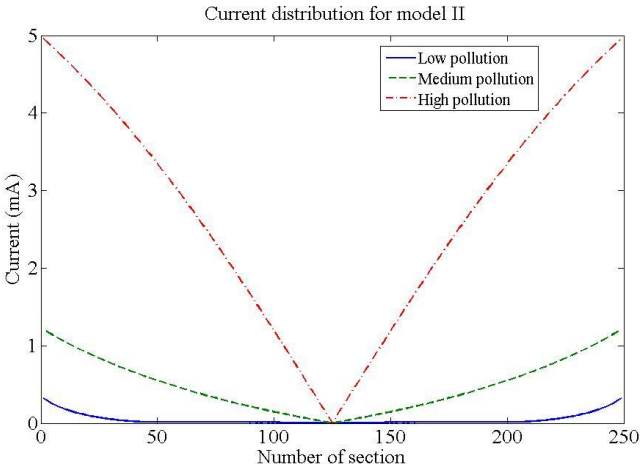

Figure. 20 Current distribution for model II

VI. CURRENT AND VOLTAGE DISTRIBUTION TREND

Variation in tower geometry varies the voltage distribution trend, but it does not vary the distribution trend of current distribution. This could be observed from the voltage and current distribution plots presented. The current distribution for both the models increases from a maximum near the tower to a minimum at the middle of the span. However, the trend followed by the voltage distribution is different from that of model II. From the results obtained from the above mentioned method, it is clear that the level of pollution influences the current distribution. In both the models regardless of the tower geometry, current increases with increase in pollution level. From the distribution calculations, one can identify the voltage and current available to create dry band arcs on the surface of ADSS cable. References [19], [23] and [25] talks about voltage and current distribution on

Table. 6 Open circuit voltage, short circuit current and power in the system

Model I			
Pollution level	***Open circuit voltage***	***Short circuit current***	***Power***
Low (10^7 Ω/m)	-0.221+j.30.114 kV	-0.345+j 0.366 mA	10.94 W
Medium (10^6 Ω/m)	-7.69+j 32.062 kV	-1.511+j 0.952 mA	18.91 W
High (10^5 Ω/m)	-22.657+j 21.097 kV	-5.575-j 0.028 mA	126.90 W
Model II			
Pollution level	***Open circuit voltage***	***Short circuit current***	***Power***
Low (10^7 Ω/m)	-9.158 + j 18.169 kV	-0.303+j 0.112 mA	0.735 W
Medium (10^6 Ω/m)	-8.75 +j 21.811 kV	-1.106 +j 0.491mA	1.043 W
High (10^5 Ω/m)	-21.051 +j 19.148 kV	-4.959- j 0.076 mA	105.837 W

the surface of ADSS cable for different configuration.

In spite of these calculations and proper placement, the cables tend to fail after a certain number of years due to aging and due to the inaccuracy of predicting dry band arcing. In this chapter, a slightly modified experimental setup and the results of the experimental setup indicating the power developed during the arcing is shown.

VII. PROPOSED CALCULATION METHODOLOGY

For all the experiments performed, the samples were prepared from the same model. Figure. 21 show the electrical circuit used for measuring the power drop across the arc in testing ADSS cables. The output from the high voltage end of the transformer is connected to a potential transformer. The output from the low voltage end of the potential transformer is connected to a LABVIEW measurement system. The LABVIEW system used has a sampling rate of 10k samples per second. A high voltage resistor of resistance 400MOhm and a capacitor of capacitance 650pF are connected in between the high voltage electrode and the output from high voltage output of the transformer. This is indicated by the resistor R1 and R2 is 1kOhm resistor across which the leakage current was measured. Two different circuits were used in the experiment. One with a 650pF capacitor in the circuit and the second without the capacitor. The power drop across the arc is given by (21) and (24) respectively.

(a) Power drop across the arc for the circuit with the capacitor

$$Vin = I \cdot R1 + I \cdot R2 + voltage\ across\ the\ arc + \frac{1}{c} \cdot \int I\, dt \qquad (19)$$

$$Voltage\ across\ the\ arc = Vin - I \cdot R1 - I \cdot R2 - \frac{1}{c} \cdot \int I\,dt \quad (20)$$

$$Power\ drop\ across\ the\ arc = Voltage\ across\ the\ arc \cdot I \quad (21)$$

Where

Vin = supply voltage

I = leakage current

R1, R2 = Resistors

(b) Power drop across the arc for the circuit without the capacitor

$$Vin = I \cdot (R1) + I \cdot (R2) + voltage\ drop\ in\ the\ arc \quad (22)$$

$$Voltage\ drop\ in\ the\ arc = Vin - I \cdot (R1) + I \cdot (R2) \quad (23)$$

$$Power\ drop\ across\ the\ arc = Voltage\ drop\ in\ the\ arc \cdot I \quad (24)$$

The arc discharge causes damage to the outer layer of the ADSS cable. The damage caused is thermal in nature. This experimental setup could be used to measure the power drop across the arc and to rate the cable accordingly. Figure. 22, Figure. 23, Figure. 26 and Figure. 27 indicate the supply voltage, leakage current observed for both the circuits. Figure. 24, Figure. 25, Figure. 27 and Figure. 28 indicate the calculated voltage across the arc and power calculated using (21) and (24). Figure. 25 and Figure. 28 are used to calculate the energy needed by the arc to deteriorate ADSS cable surface.

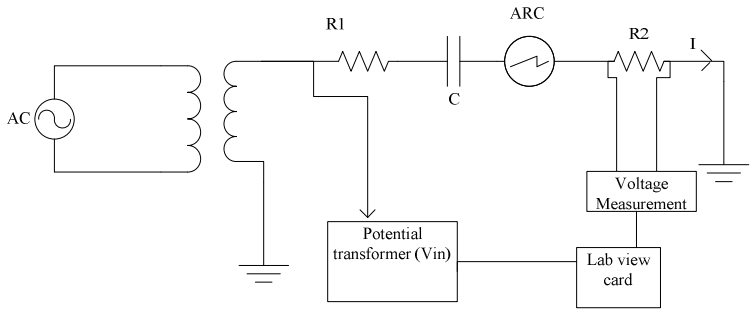

Figure. 21 Circuit used to calculate the power drop across the arc

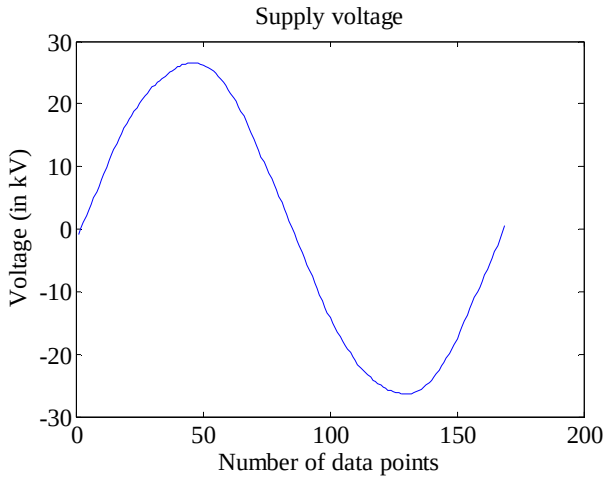

Figure. 22 Supply Voltage for the circuit with capacitor

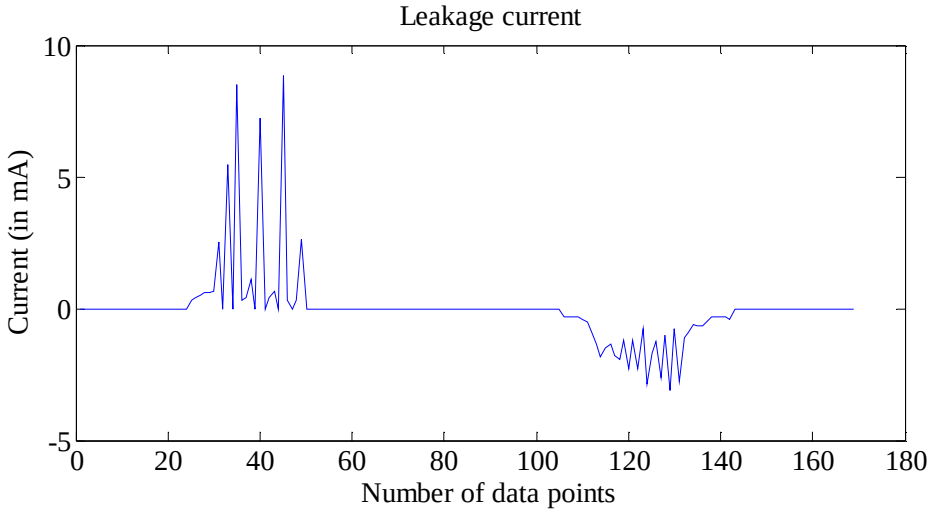

Figure. 23 Leakage current flowing in the circuit with capacitor

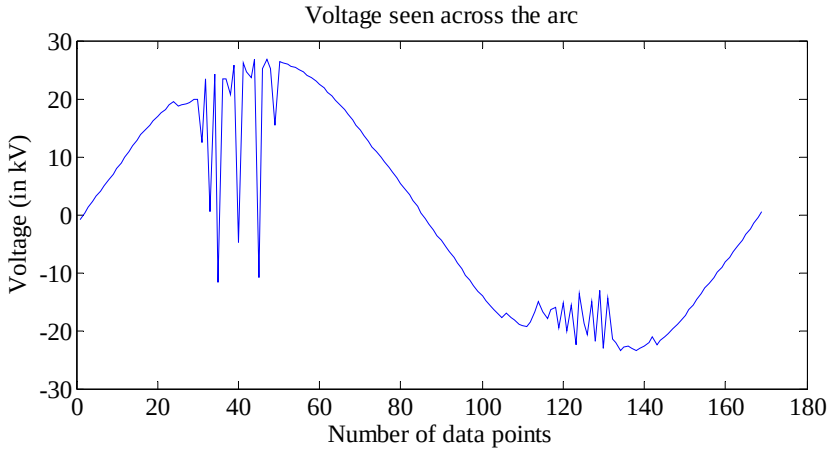

Figure. 24 Voltage across the arc for the circuit with capacitor

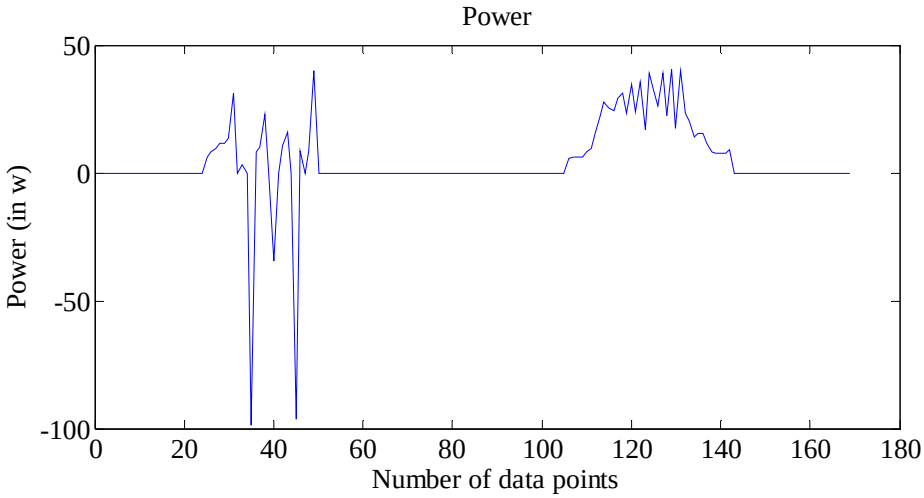

Figure. 25 Power drop across the arc for the circuit with capacitor

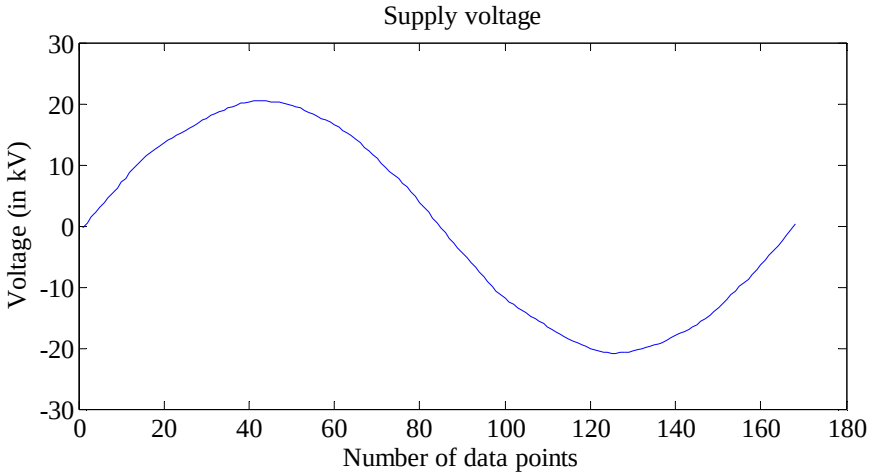

Figure. 26 Source voltage for the circuit without capacitor

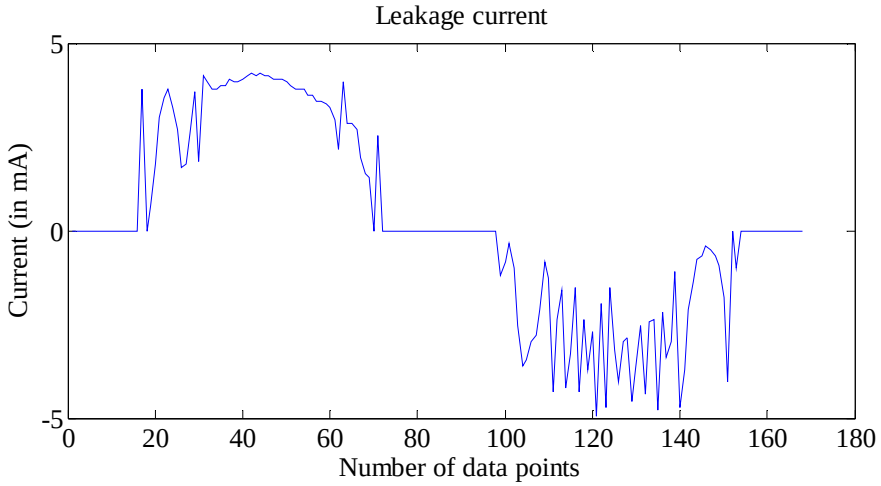

Figure. 27 Leakage current flowing in the circuit without the capacitor

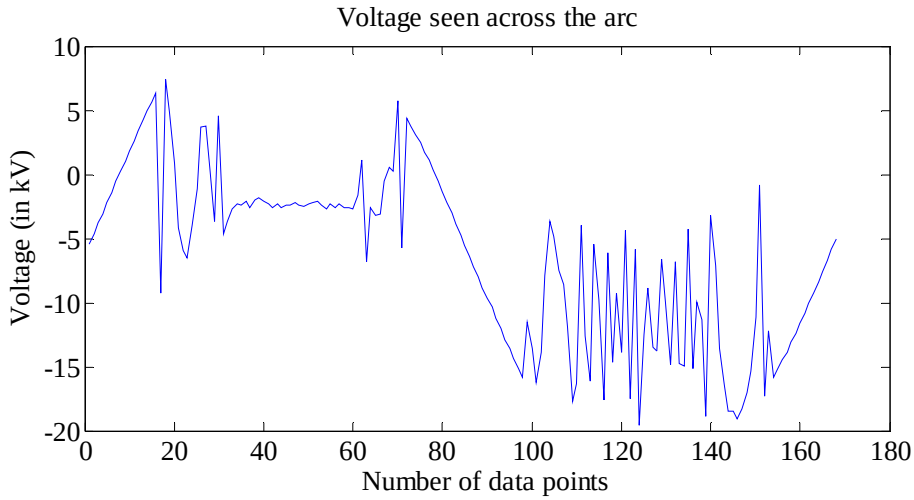

Figure. 28 Voltage across the arc for the circuit without capacitor

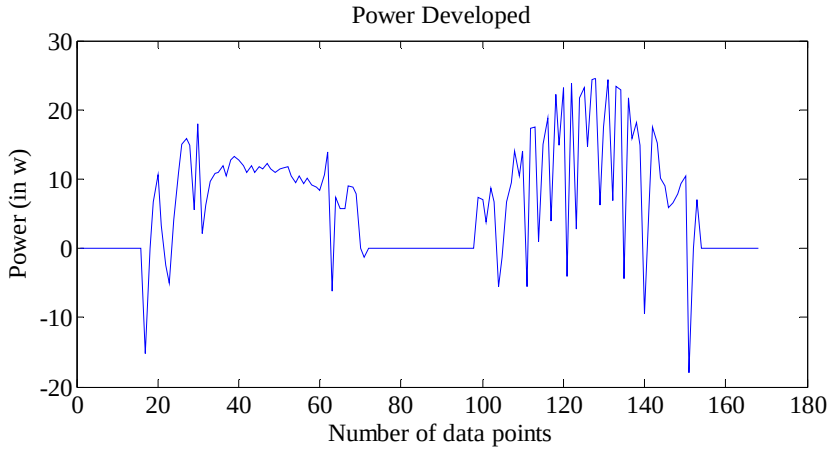

Figure. 29 Power drop across the arc for the circuit without capacitor

VIII. CLASSIFICATION OF ADSS CABLE RANKING

The recorded experimental data are used to calculate the power developed during the dry band arcing. (20) and (23) are used to calculate the power values. Supply voltage, leakage current, voltage across the arc and power across the arc for the experiments performed with and without the capacitor are shown from Figure. 22 to Figure. 29. Table. 6 shows the power available in the system to create dry band arcing. Table. 7 and Table. 8 indicate the power developed during the deterioration of the cable surface.Table. 8 is used for the evaluation, as Table.

8 corresponds to the experiments carried out with an RC bank and this is a good model which is more analogous to the capacitive coupling in the field. Experimental results when evaluated against the results from Table. 5 indicate that the power in the system for low and medium pollution is less than the power observed during the experiments for surface deterioration. This indicates the cable will survive at low and medium pollution in both the models. But, the power in the system for high pollution level is higher when compared to the power observed during the experiments for surface deterioration. The cable will not survive high pollution in both the models as the power available in the system is more than what it is needed to deteriorate the surface of ADSS cable sheath.

Table. 7 Energy developed in the arc for circuit with capacitor – (a)

Cycle	**Energy (in Joules per cycle)**	**Power (W)**
1	0.1473	6.2006
2	0.1635	16.3420
3	0.1643	18.7296
4	0.2	26.065
5	0.0879	26.4343
6	0.0729	27.4379
7	0.0735	25.6385
8	0.0589	16.166
9	0.0495	21.5225
10	0.0486	19.6565
Average		20.41

Table. 8 Energy and power developed in the arc for circuit without capacitor – (b)

Cycle	Energy (in Joules per cycle)	Power (W)
1	0.1768	14.4664
2	0.168	14.5975
3	0.1463	12.2043
4	0.1255	12.6366
5	0.101	10.5059
6	0.1596	12.0043
7	0.0979	7.2922
8	0.1496	12.7765
9	0.1047	10.0883
Average		11.84

Chapter 4

Experimental study on dry band arcing

I. INTRODUCTION

The experimental setup used to study dry band arcing is explained in detail in this chapter. Reasoning of the experimental setup and the methodology used to conduct the experiment are justified by comparing the methodology with dry band arcs occurring in the field. Sample preparation and the samples used for the tests are presented. Finally, the chapter is concluded with the failed samples showing damage due to arcing.

II. EXPERIMENTAL SETUP

A. Equivalent circuit representation of transmission lines and ADSS cable

As mentioned earlier, the outer cable sheath of ADSS cables when manufactured is hydrophobic in nature and is arc resistant. The ADSS cable is coupled to the conductors, earth wire and the ground by distributed capacitance throughout the entire span of the transmission line. Pollution that settles on the non-conductive layer of the ADSS cable can be considered as resistances between the distributed capacitance. This resistance varies with the amount of pollution deposited on the cable layer. Figure. 30 show the capacitive coupling that exists between the transmission line and ADSS cable. The above mentioned phenomenon was reviewed in detail in chapter 2 and chapter 3.

There will be a leakage current flowing on the resistive layer due to the capacitive coupling between transmission lines and the cable. This leakage current along with ultra violet radiation and pollution aids in early aging of cable

sheath and makes the cable sheath less hydrophobic. When the cable is hydrophobic and resists moisture on the layer, dry band is never prominent. At places like Phoenix, where the presence of moisture is very less, dry band arcing is not prominent. But, occurrence of dry band will increase in the presence of moisture and as the cable gets more hydrophilic and less hydrophobic. Studies have been conducted on ADSS cables which were working in highly polluted environment and in places with such pollution level, their outer layer showed resistance of very low value.

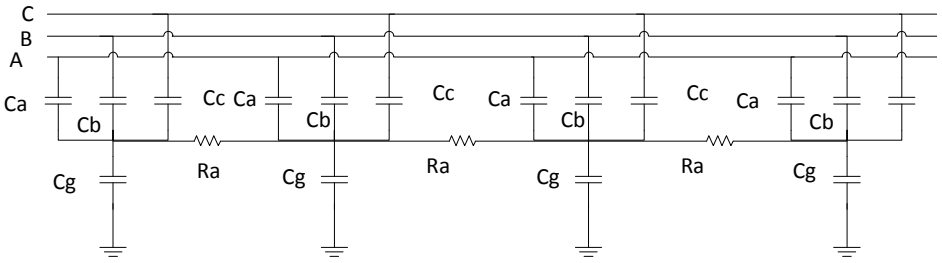

Figure. 30 Capacitive coupling for a three phase single circuit line

Table. 9 Typical Resistance and capacitance values used in experiments

Pollution	Resistance (Mohms)	Capacitance (pF)
10^5	4.2	650
$10^{5.7}$	5.8	457
10^6	13.1	200

Typical space potential available for arcing is around 15 to 25 kV, which was shown in chapter 2 and chapter 3. This voltage level depends on various factors like the working voltage level of the transmission line, pollution available in the environment, relative sag between cable and transmission line. Figure. 30

show the three phases A, B, C and the capacitive coupling between the phases and the cable. Ra in Figure. 30 indicates the conductive moist pollution layer that settles down on the outer cable sheath. Table. 9 shows typical values of Ra considered for different pollution levels.

The experimental setup used in testing has an RC impedance to simulate the effect of pollution during cable tests. Figure. 31 shows the experimental setup used for testing ADSS cables. An RC circuit is connected in between the high voltage electrode and high voltage supply. The high voltage electrode is connected to one end of the sample and the other end of the sample is connected to the ground through a series resistor. The leakage current flowing through the test circuit is measured from the voltage across the 100 ohm series resistor. For all the experimental work carried out in this thesis, cables from the same manufacturer and same model were used.

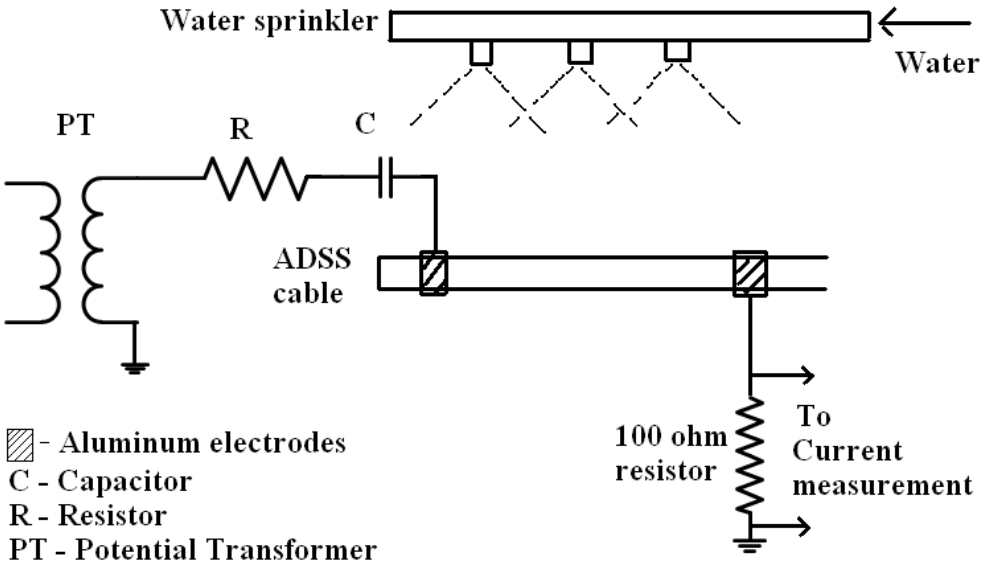

Figure. 31 Experimental setup used in testing ADSS cables

B. Mechanism of dry band arcing

The mechanism of dry band arcing under field conditions are explained here to provide a correlation between the methodology used in the experimental setup and dry band arcing in the field. Dry band arcs typically start to occur when the accumulated pollution layer on the outer cable sheath gets moist. When the cable sheath accumulates moisture on its outer layer, the high resistive pollution layer becomes conductive and leakage current starts flowing through the layer. As long as this leakage current flow is uninterrupted, arcing does not occur. As long as moisture is available and provides a conductive path for the flow of leakage current, dry bands will not be formed. The moisture is available because of the presence of rain and dew in the environment. When rain stops, the moisture will dry either due to the heat from the sun or due to heat developed during the leakage current flow. The leakage current flow on the surface of the cable produces a Joules heating effect and begins to dry the cable out [26].This is correlated using the experiment in the upcoming section.

When the cable layer dries up due to the leakage current flow, dry bands will be formed on the cable's outer sheath. If the available voltage across this dry band is high enough, arcs will be formed [3]. This is explained in Figure. 32. The cable layer will be damaged when the nature of the arc is stable. The aim of the experiment is to simulate this environment in the lab. The following two factors should be satisfied by the experimental methodology

- a moist conductive layer
- formation of dry bands on the surface of cable

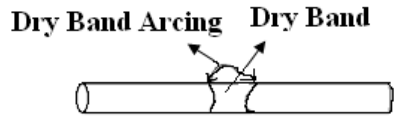

Figure. 32 Formation of dry band arcing

C. Simulation of dry band arcing using the experimental setup

The experiments are conducted in such a way that they simulate the real environment needed to start dry band arcs. This is also explained in Figure. 34. The cable samples are tested at a starting base value of 5 kV. Water is sprinkled over the cable samples between the electrodes as shown in Figure. 31. Water used for the experiments has salinity of 1% in it. This is used to simulate the conductive moist layer. To facilitate an even distribution of water droplets over the cable surface, the water is sprinkled for about two minutes. The next important feature that was considered in the experiment was to simulate a way to dry the conductive layer. At the earlier stages of testing, comparatively low voltage was supplied across the electrodes and the leakage current flowing on the ADSS cable layer was very less. It will take a long time for the cable layer to dry at earlier low voltage levels when compared to a higher voltage level. On the other hand, during the beginning of the experiment, the hydrophobicity of the cable layer will be high and the water droplets will move down and eventually fall off the cable layer due to gravitational force. The time allowed to dry is made sure that it is not too long and also not short and is selected as thirteen minutes for the experiments carried out. The entire cycle will take fifteen minutes combining a two minute wetting period with thirteen minutes drying period.

The samples tested using the setup will have a voltage of 5 kV applied at the beginning. If the sample survives the first cycle of fifteen minutes without any damage to the outer sheath, the voltage applied will be incremented by 5 kV and the sample will be tested for another cycle. The experiment will be continued on the cable sample with an increments of 5kV till the cable sample fails. A timer is used to start and stop the pump supplying the misting devices. Figure. 33 shows the timer used in the experimental setup. The copper sheets in the timer will turn on the pump when it touches the switch and when the copper sheets are not touching the switch the pump will be turned off. Figure. 34 (a) shows a cable sample being testes using the setup. Figure. 34 (b) shows the presence of conductive waterlayer on the surface layer. When the sample is allowed to dry, that is, when the pump supplying the misting devices is turned off, the moist layer dries due to the leakage current flow. As shown in Figure. 34 dry bands will be formed unevenly and the dry band formed is similar to the ones observed in the field and the applied voltage will be distributed across this dry band. Arcs were formed across these dry bands and this is shown in pictures from Figure. 34 (c) to Figure. 34 (f). The heat developed due to the dry band arc destroyed the outer cable sheath.

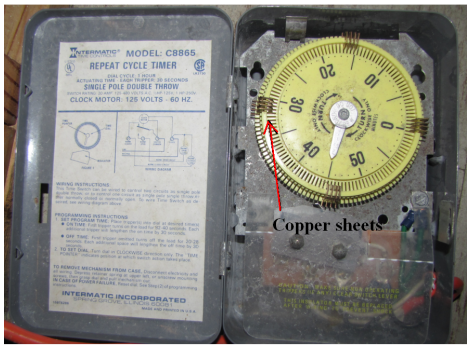

Figure. 33 Timer showing copper sheets

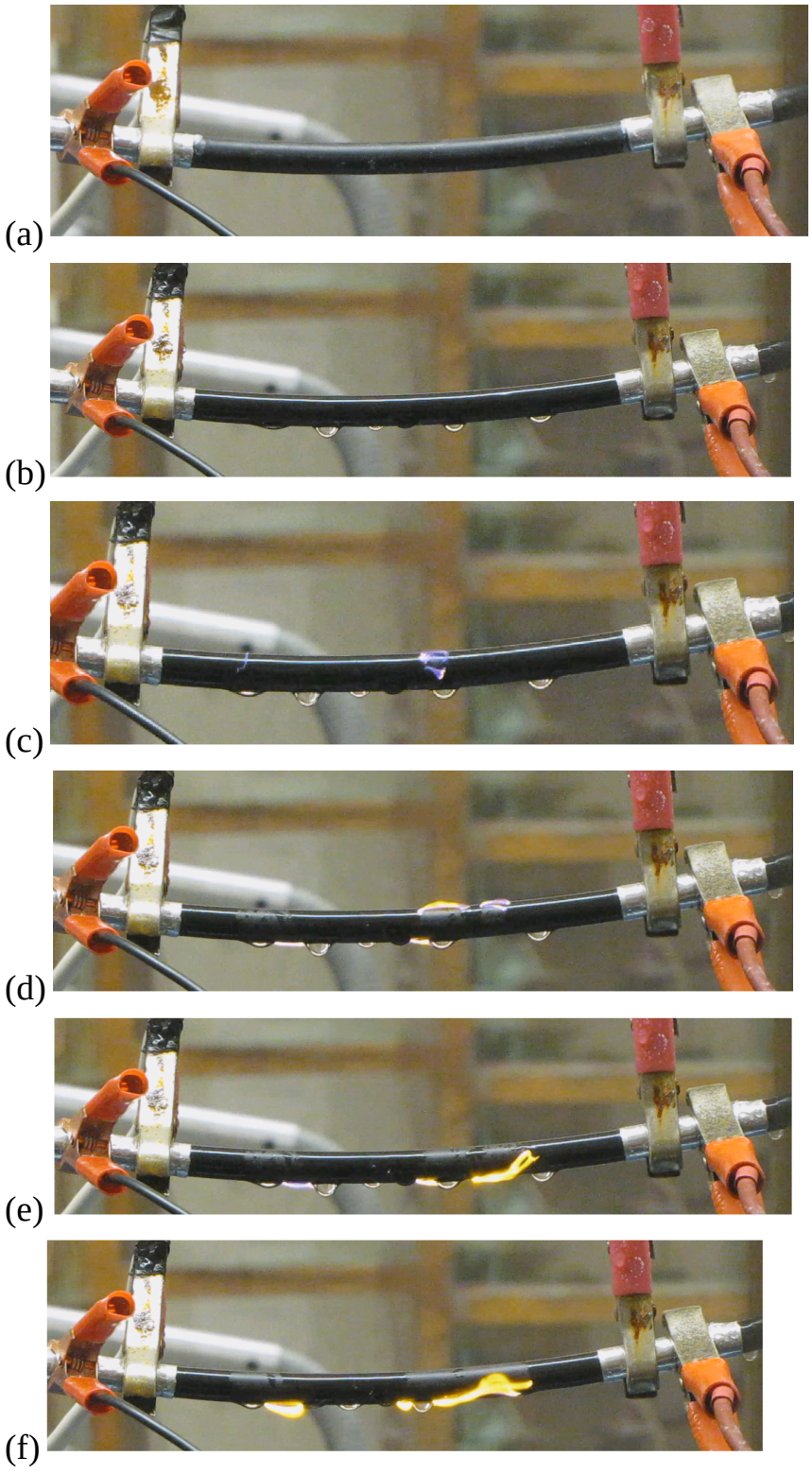

Figure. 34 Working of the experimental setup

D. Sample preparation

The same setup and methodology is used to compare the effect of dampers on dry band arcing and also for the experiments carried out to calculate the power developed during dry band arc. Table. 9 show the typical RC values used in the experiments. For the experiments conducted, high pollution is considered, resistors of equivalent resistance 4.2 Mohm and capacitors of equivalent capacitance 650 pF were used for the RC bank.

When the cable is used for testing without the damper, the cable is cut into samples of 18 inches in length and the ends of the cable are sealed to prevent moisture from entering the fiber inside the cable. Aluminum electrodes are used and a distance of six inches is kept between the aluminum electrodes. The same electrodes setup is used when the dampers alone are tested. But, when the cable in the presence of damper is tested, the cable is strung between the cage ends and the damper is installed over it. Aluminum electrodes are placed over both the damper and cable and are shown in Figure. 34.

E. Performance of the samples

The performance of the samples when tested in the setup as mentioned above is given in Table. 10, Table. 12 and Table. 11. It could be observed that the cable sample in the absence of damper withstood four cycles and failed during the fifth cycle. When damper is installed over the cable, the sample withstood two cycles and failed in the third cycle. This is due to the fact that ADSS cable sample when tested in the absence of damper aged at a slower rate than the damper sample and ADSS cable with damper on it. The hydrophobicity of the cable was re-

duced at a slower rate than the damper sample and ADSS cable sample with damper on it. The failed samples are shown in Figure. 35, Figure. 37 and Figure. 36. The leakage current measurements made on the samples are shown in the next chapter with their corresponding hydrophobicity.

Table. 10 Performance of cable sample

Applied voltage	**Status of the cable sample**
5 kV	Undamaged
10 kV	Undamaged
15 kV	Undamaged
20kV	Undamaged
25 kV	Damaged

Table. 12 Performance of cable sample when damper is installed

Applied voltage	**Status of cable and damper**
5 kV	Undamaged
10 kV	Undamaged
15 kV	Damaged

Table. 11 Performance of damper

Applied voltage	**Status of damper sample**
5 kV	Undamaged
10 kV	Undamaged
15 kV	Damaged

Figure. 35 Cable sample showing damaged outer sheath

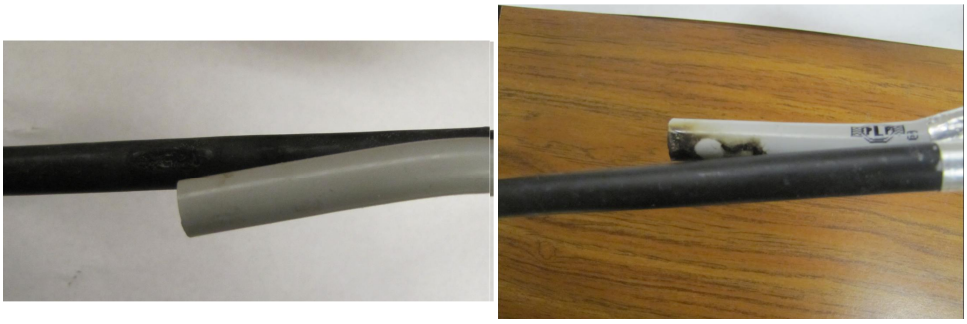

Figure. 36 Sample showing damage on the outer layer when damper is installed over the cable

Figure. 37 Damper sample showing damage in the outer sheath

Chapter 5

Hydrophobic nature and leakage current flow on the samples

I. INTRODUCTION

This chapter is divided into two sections, the first talks about the hydrophobic nature of the sample and the second talks about the leakage current flow on the surface of the samples during experiments. Also, the importance of contact angle on hydrophobicity of the samples and the contact angle for the fresh samples and the samples after the experiments is presented. Finally, a comparison is made between the leakage current on surface of the samples.

II. GUIDELINES FOR HYDROPHOBICITY CLASS

Dielectrics and electrical insulation society (DEIS), a society of the institute of electrical and electronics engineers (IEEE) has a dedicated standard IEEE 1523 – IEEE guide for the application, maintenance and evaluation of room temperature vulcanizing (RTV) silicone rubber coatings for outdoor ceramic insulators [27]. In this standard, a hydrophobicity classification guide has been included. In this guide, composite insulators and coated insulators are classified into

Table. 13 Contact angle and its relation with other physical parameters

Contact angle	**Small**	**Large**
Wettability	Good	Bad
Adhesiveness	Good	Bad
Hydrophobic nature	Bad	Good
Hydrophilic nature	Bad	Bad

seven classes of hydrophobicity. Class HC 1 indicates that the hydrophobicity of the insulator sample is highly hydrophobic in nature and the class specification extends to HC 7, where HC 7 indicates a completely hydrophilic surface. Figure. 38 show the seven classes.

III. CONTACT ANGLE – A MEASURE OF HYDROPHOBICITY

When a liquid or vapor interface meets a solid surface, the angle formed between the solid surface and the tangent line to the upper surface at the end point is called contact angle. This contact angle could be a measure of adhesion, wettability and also the hydrophobicity of a surface. Table. 13 shows the relationship of contact angle with the above mentioned physical parameters. It could be inferred from the table that contact angle could be a measure of hydrophobicity or

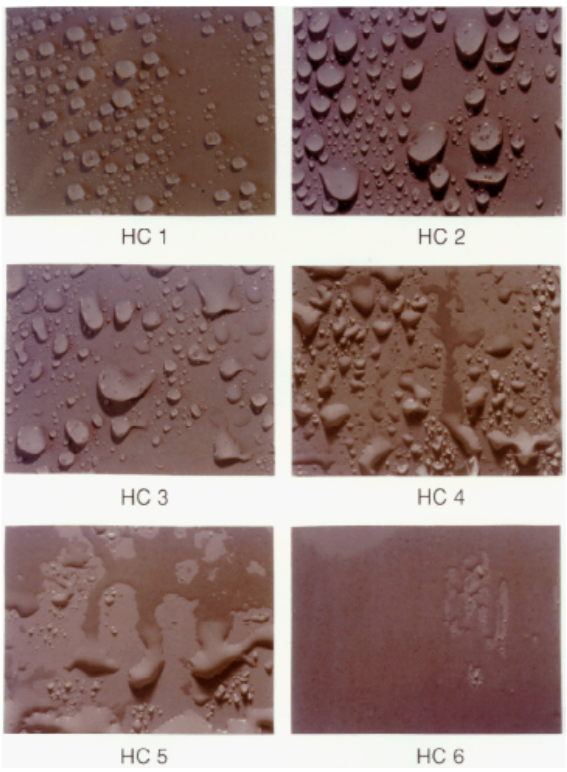

Figure. 38 Hydrophobicity classes of outdoor insulators

hydrophilicity of a material. Figure. 39 (a) and (b) shows the contact angles at the surface of a hydrophobic and hydrophilic material.

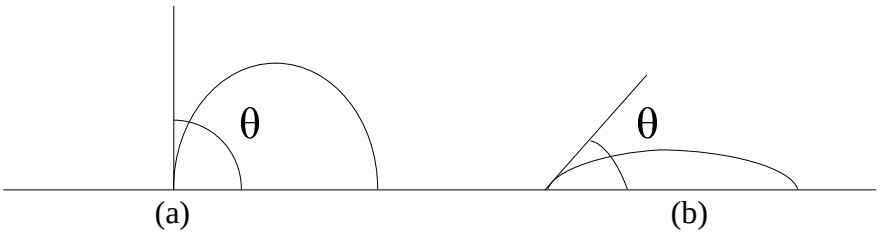

Figure. 39 Contact angles of hydrophobic and hydrophilic surfaces

IV. CONTACT ANGLES FOR DIFFERENT SURFACES

The hydrophobicity of the insulating material can be measured by the contact angle between the surface of the water droplet and the insulating material surface. Figure. 39 (a) shows the contact angle for a hydrophobic material and it is near 90 degrees. Figure. 39 (b) shows the contact angle for a hydrophilic material and it is between 20 to 40 degrees. When the damper ages and also when pollution settles on the surface of the cable, the hydrophobicity of the damper varies and the contact angle will change.

V. CONTACT ANGLE ON THE SURFACE OF THE SAMPLES

Figure. 41 (a) and (b) show the contact angle of the water droplet on the damper sample and cable sample. It could be observed that the samples are not perfectly hydrophobic material. Figure. 40 (a) and (b) show the damper sample and cable sample after the sample were failed. It could be observed that the sample surfaces are less hydrophobic now. The contact angle has decreased from what it was when the samples were tested.

(a) (b)

Figure. 41 Fresh samples of damper and cable

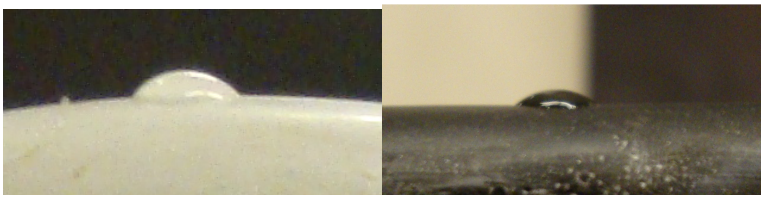

(a) (b)

Figure. 40 Contact angles of failed samples

VI. EXPERIMENTAL SETUP AND METHODOLOGY FOR TESTING DAMPER

The experimental setup explained in chapter 4 is used to test the dampers. The methodology is the same to have uniformity in the tests. A fresh sample of SVD is used for testing. The electrodes are kept six inches apart in the middle of the sample. The voltage applied starts from 5 kV and it increases in increments of five till the damper burns. The water solution used has 1% salinity. Table I shows the observations made during the tests.

VII. EXPERIMENTS ON DAMPER

The samples used here are spiral vibration dampers made for ADSS cables. The voltage applied is increased from 5 kV till there is burning on the cable surface. Figure. 42, Figure. 43 and Figure. 44 show the surface of the damper at different voltage levels. Figure. 42 show that when 5 kV was applied the surface of the damper was hydrophobic. Voltage applied was kept at 5 kV for fifteen

minutes and then the voltage level was increased to 10 kV. Figure. 43 show the surface of the damper at 10 kV.

It could be observed that the damper is less hydrophobic at the voltage

Figure. 42 Surface of the damper at 5 kV with water droplets on the surface

Figure. 43 Surface of the damper when 10 kV is applied

Figure. 44 Surface of the damper when 15 kV is applied

level of 10 kV. After fifteen minutes of operation at 10 kV the voltage was increased to 15 kV. Figure. 44 show the surface of the cable at 15 kV. The surface is hydrophilic at this voltage level. A continuous water filament could be observed on the surface of the damper. Eventually the cable started burning at the voltage level of 15 kV. The aim behind the tests on the dampers was to explain the importance of hydrophobicity of the damper in dry band arcing when it is installed over the cable. Figure. 42 show water on the damper when the samples were new and when they were tested for 5 kV. The water droplets on the damper is similar to Figure. 39 where the contact angle is near 90 degree. Figure. 43shows the damper sample when the damper was tested with 10 kV. It could be seen that the hydrophobicity is reduced.

VIII. LEAKAGE CURRENT FLOW ON THE SURFACE OF THE SAMPLES

Leakage current flow on the surface of the samples was recorded using the series resistor in the experimental circuit. Leakage current was measured whenever there is a presence of visual dry band arcing. Figure. 46 and Figure. 47 show the leakage current flow on the surface of ADSS cable sample and the cable sample with damper on it. Table II shows the maximum and minimum leakage current that was observed during the experiment.

Figure. 42, Figure. 43, and Figure. 44 showed the hydrophobicity of the samples at 5, 10 and 15 kV. This indicates that the number of cycles required by the damper to fail is less compared to the cable sample without damper, which took five cycles to fail. Leakage current details are given in Figure. 46 and Figure. 47. This indicates that the aging time of the damper and the ADSS cable differ.

Due to this, when the damper was installed over the cable and tested, the sample failed after three cycles at 15 kV. If the damper and the ADSS cable tested were to be installed together the cable will fail earlier than expected and also the damper will derate the cable. The cable sample in the absence of damper used for testing failed at 25 kV, which indicates that the cable will withstand 15 and 20 kV of applied voltage. But, the damper when installed over the cable derated the cable to 15 kV. Moreover, it could be observed from the table that the presence of damper increased the leakage current flow in the surface of the sample. When the damper is installed for an applied voltage of 15 kV the maximum observed leakage current flow is 0.8 mA which is a 100 percent increase. Figure. 45 show the arc which damaged the cable. The red mark in Figure 45 (b) shows that the presence of water droplet remaining undamaged. And also Figure. 45 show the difference in hydrophobicity between the damper and cable. The reduced hydrophobicity kept the water droplet in between the damper and cable and this created an arc and damaged the cable surface. The length of the arc which damaged the cable is around 0.7 inches in length.

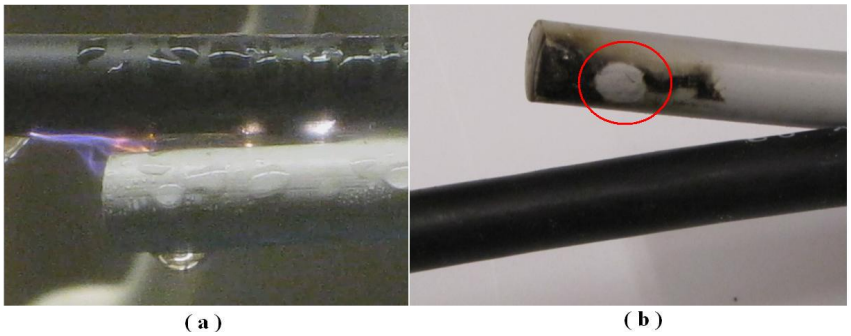

(a) (b)

Figure. 45 Samples showing damage on the damper

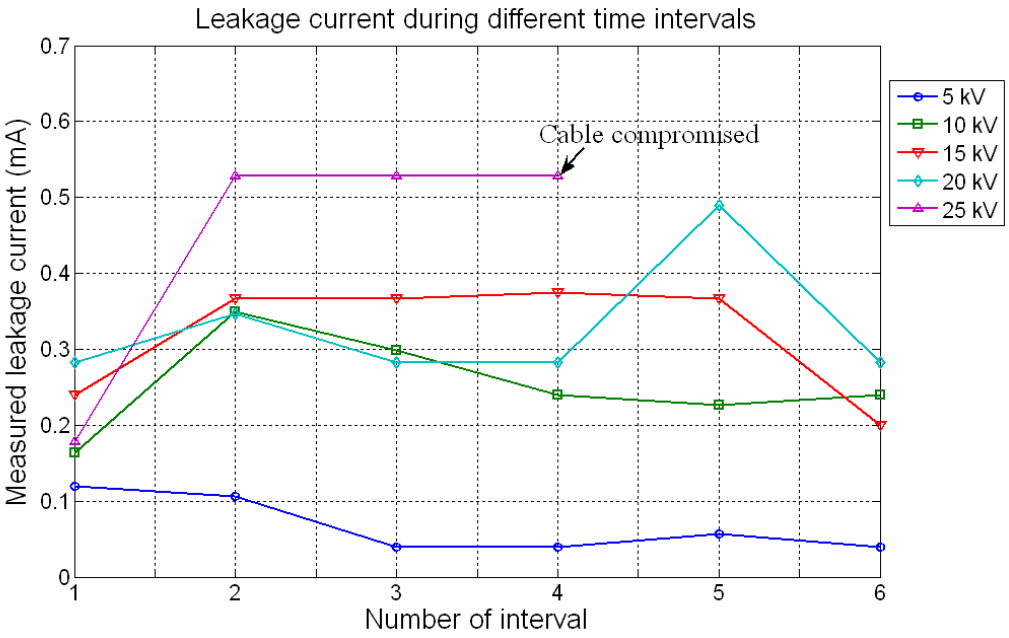

Figure. 46 Leakage current on the surface of ADSS cable

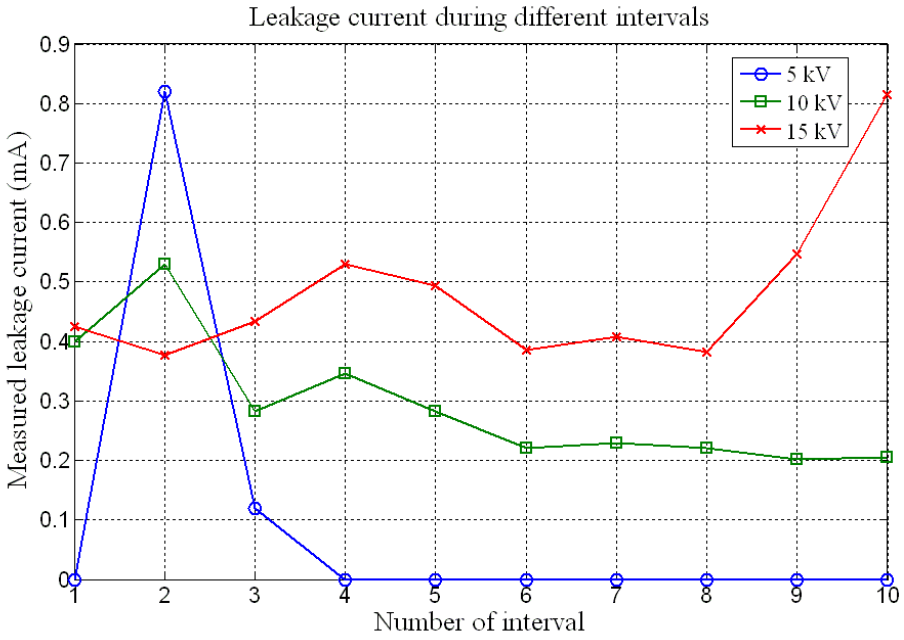

Figure. 47 Leakage current on the surface of damper and cable setup

Table. 14 Leakage current flow on the surface of samples

Applied voltage	**ADSS cable sample mA**		**Cable and damper sample mA**	
	Min	Max	Min	Max
5 kV	0.05	0.12	0	0.8
10 kV	0.18	0.24	0.2	0.3
15 kV	0.2	0.38	0.39	0.82
20 kV	0.28	0.49	-	-
25 kV	0.18	0.52	-	-

IX. SUMMARY

The criterion that was considered to say that the samples failed is a stable dry band arc which visibly burns the cable and it should change from a stable arc to a stable flame. The damper surface age very quickly when compared to the ADSS cable. The surface of the damper should be made with good hydrophobic material and with one which has a very long aging time. If this damper is used with an ADSS cable which has a better hydrophobic properties and longer aging time, the damper will reduce the characteristics of the cable properties. This can reduce the aging time of the cable. Moreover, even if the cable was rated for 25 kV, because the damper burns at 15 kV the cable will also burn at 15 kV. The above tested sample, if installed along a cable which was rated at 25 kV and installed at a field of 20 kV will create dry band arcing and damage the cable even though the cable was rated at 25 kV.

The selection criteria of damper should not only be limited to outer diameter of the cable, span between the towers but also the electrical performance of both damper and the cable. It is suggested by the manufacturers that moving dampers to the middle of the span will reduce dry band arcing on dampers as the magnitude of leakage current is less. But, this might affect the damping properties of spiral vibration dampers. A proper decision would be to test the dampers and rate them according to their electrical performance and install them on cables which have similar electrical properties.

Chapter 7

Computer simulation of ADSS cable and damper

I. INTRODUCTION

In the previous chapter, effect of damper on ADSS cable is shown by comparing the leakage current flow on the surface of the ADSS cable and a conclusion based on the hydrophobicity of the samples is presented. In this chapter, electric field on the surface of the ADSS cable is simulated. A comparison between the surface electric field for different samples is shown.

II. DETAILS OF SIMULATION MODELS

Software packages based on finite element, finite difference, boundary element and charge simulation methods are commercially available for electric field simulation. For the work presented in this chapter, a software package based on boundary element analysis method called as COULOMB is used. The samples that are used in the experiments and some of the characteristics of the experiment are modeled in the simulation. The electric field distribution in between the electrodes is of interest here.

A. Basic models used for simulation

The models used in the COULOMB simulation are the following

i. ADSS cable sample without damper and water strip
ii. ADSS cable sample with damper but without water strip
iii. ADSS cable sample with damper but without water strip
iv. ADSS cable sample with damper and water strip

B. Description of the models

The following details of the ADSS cable were included in the models used

i. Central strength member

ii. Optical fiber

iii. Outer dielectric sheath

iv. Aluminum electrodes and

v. Dielectric damper

Some of the materials used to manufacture the cable were not provided in the software materials library. For materials that were not available in the software, their corresponding relative permittivity was used to model them in the simulation. Details of the materials used in the simulation are given in Table. 15.

Table. 15 Relative permittivity of the materials used

	Material used	**Permittivity**
Buffers and fillers	polybutyleneterapthalate	2.45
Center strength member	Reinforced plastic	3.7
Outer sheath	Polyethylene	2.25
Electrodes	Aluminum	1
Damper	Polyvinylchloride	4.5
Water strip	Water	80.2

C. Dimensions of the samples used

The dimensions of the samples used in the experimental testing were used as the base for the COULOMB models. COULOMB model has ADSS cable of length 9 inches. The electrodes are of length 1.5 inches. The electrodes are spaced at a distance of six inches. The water strip used in the models is of length 2.5 inches. The presence of water strip simulates the situation when the surface of the samples becomes less hydrophobic. The specifications of the models are shown in Table. 16. and are the generic details of the COULOMB samples used throughout

Table. 16 Specification of the sample

	Radius in inches
Buffers and fillers	0.0118124
Center strength member	0.09845
Outer sheath Inner radius	0.3399
Outer sheath outer radius	0.4384
Cable electrode inner radius	0.4484
Cable electrode outer radius	0.4583
Damper radius	0.3837
Water strip inner radius (over the damper)	0.3937
Water strip outer radius (over the damper)	0.4219
Damper electrode inner radius	0.3864
Damper electrode outer radius	0.3964
Water strip inner radius (over the cable)	0.448425
Water strip outer radius (over the cable)	0.476665

this study. The models used in the simulation are made close to the samples used in the experiment.

III. ELECTRIC FIELD SIMULATION ON THE SURFACE OF THE MODELS

A. Case I – Cable model without damper without water strip

The model without water strip could be called as a dry model because this represents the ADSS cable without any conductive moist pollution on its layer. Electric field on the surface of this when compared with model which has water strip over it provides a good understanding of the phenomenon. Figure. 48 shows the model used in COULOMB simulation. It shows the fiber optics inside the cable, a central strength member and an outer dielectric sheath. The tubes at two ends of the model represent the aluminum electrodes. It could be observed from the surface electric field plot that near the electrodes the electric field distribution is higher, which increases the possibility of breakdown of air near the electrodes. Towards the ground, electric field distribution reduces to a very low value and there is a small spike near the ground electrodes.

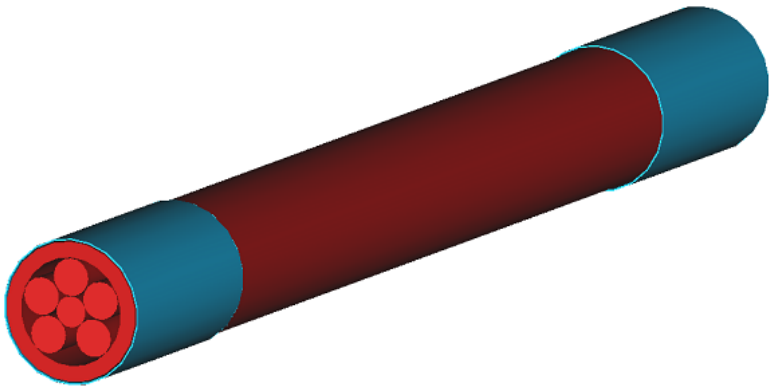

Figure. 48 COULOMB model for case I

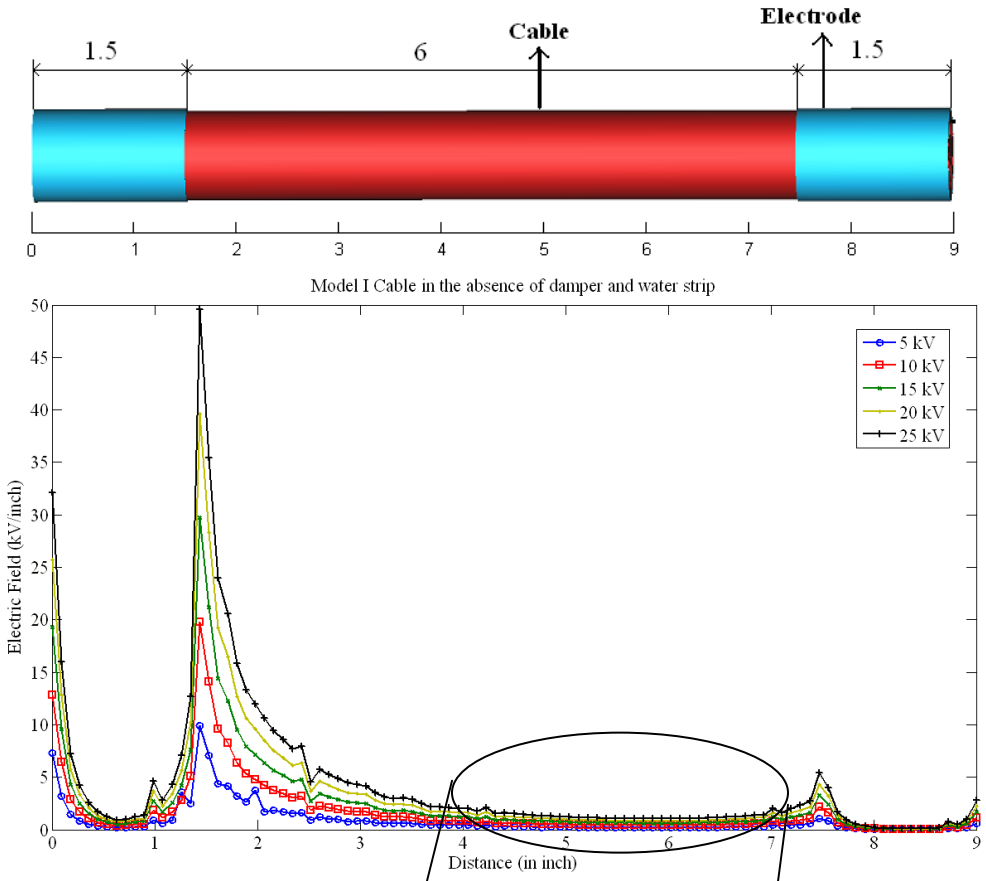

Figure. 49 Electric field on the surface of the cable for model I

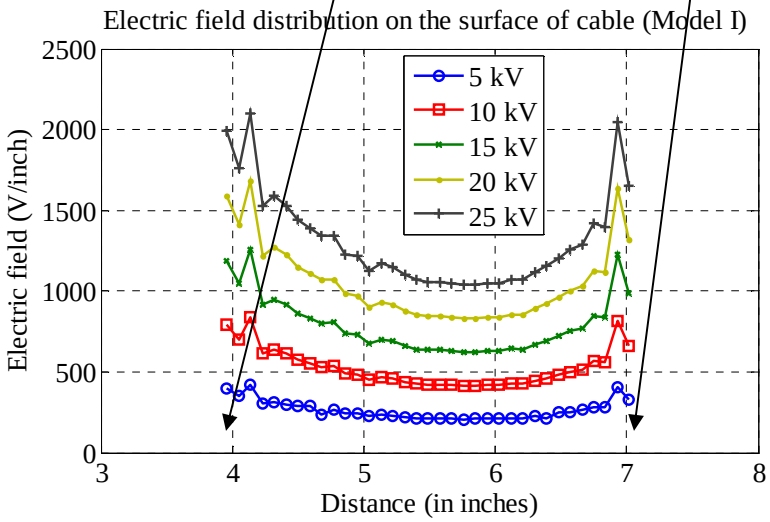

Figure. 50 Electric field for Model I between 4 and 7 inches from high voltage electrode

B. Case II – Cable model in the absence of damper, with water strip

In this model, a water strip is placed over the cable outer sheath. The water strip starts at 4.5 inches and ends at 7 inches from high voltage electrode end of the sample. The specifications and details of the materials used in the sample are given in Table. 15 and Table. 16. It could be observed that at 4.5 inches where the water strip begins there is a small increase in the electric field and also at 7 inches where the water strip ends. This model is used to compare the effect of water strip present over the damper on the electric field distribution.

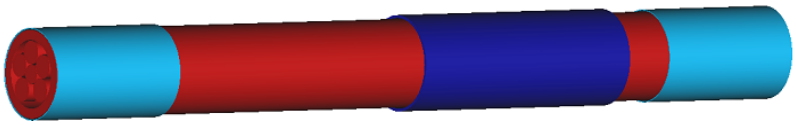

Figure. 51 COULOMB model for case II

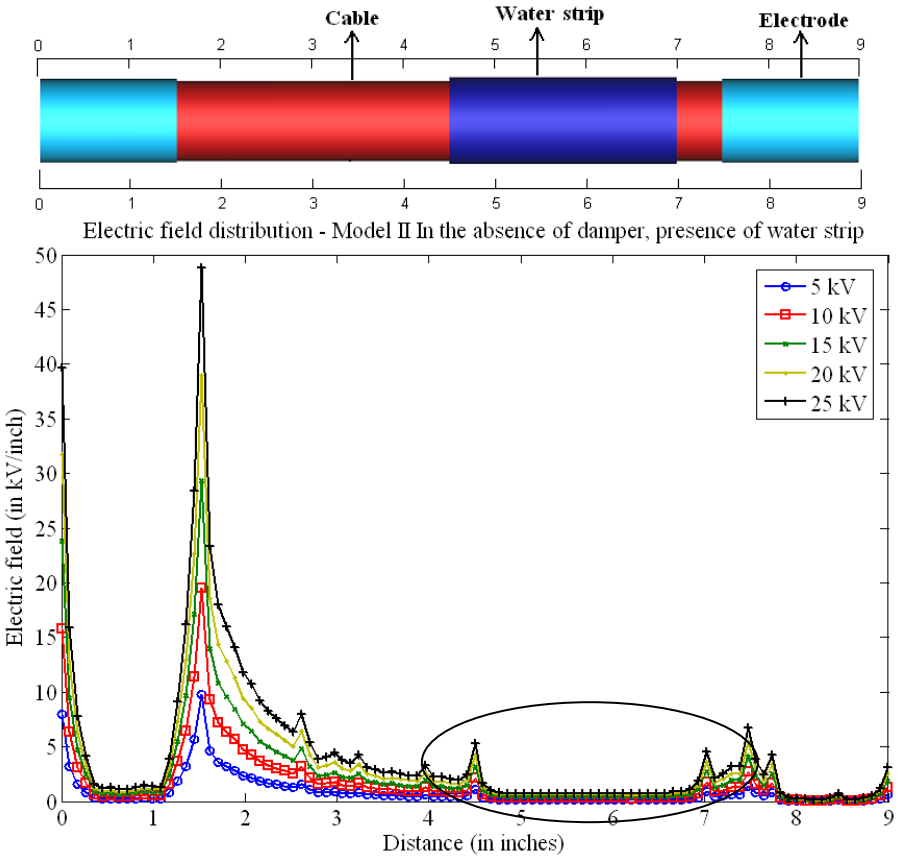

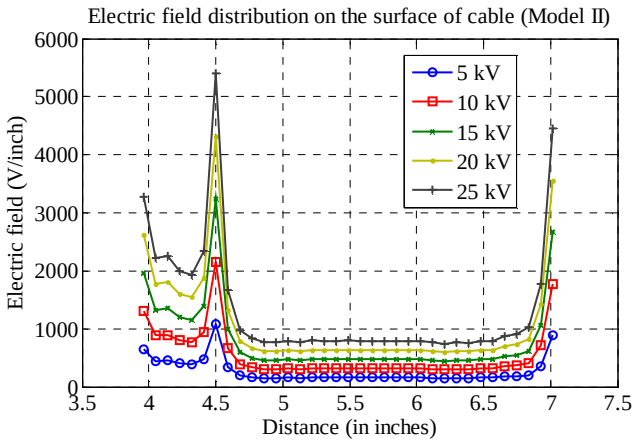

Figure. 53 Electric field for Model II between 4 and 7 inches from high voltage electrode

C. Case III – Cable model with damper, in the absence of water strip

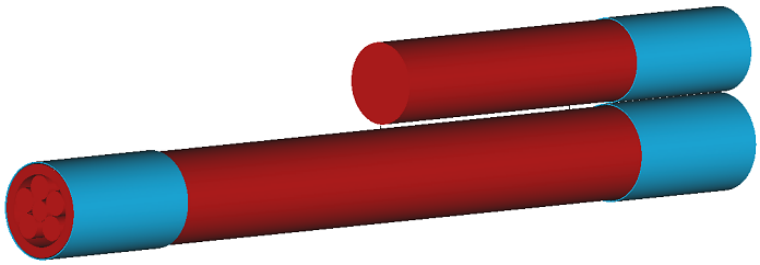

Figure. 54 Coulomb model for case III

Figure. 54 shows the COULOMB model used to simulate the case with damper over the cable and in the absence of water strip. The damper is placed above the cable at a distance of 4.5 inches from the high voltage electrode till the end at 9 inches. COULOMB generates an error when two surfaces overlap, the surfaces of the models shown in the simulation does not touch each other. Due to this, another grounding electrode is placed over the damper. Poly vinyl chloride (PVC) is the material used to simulate the damper. Electric field on the surface of the cable did not change much from case I. The presence of damper did not make any difference in the electric field under dry conditions.

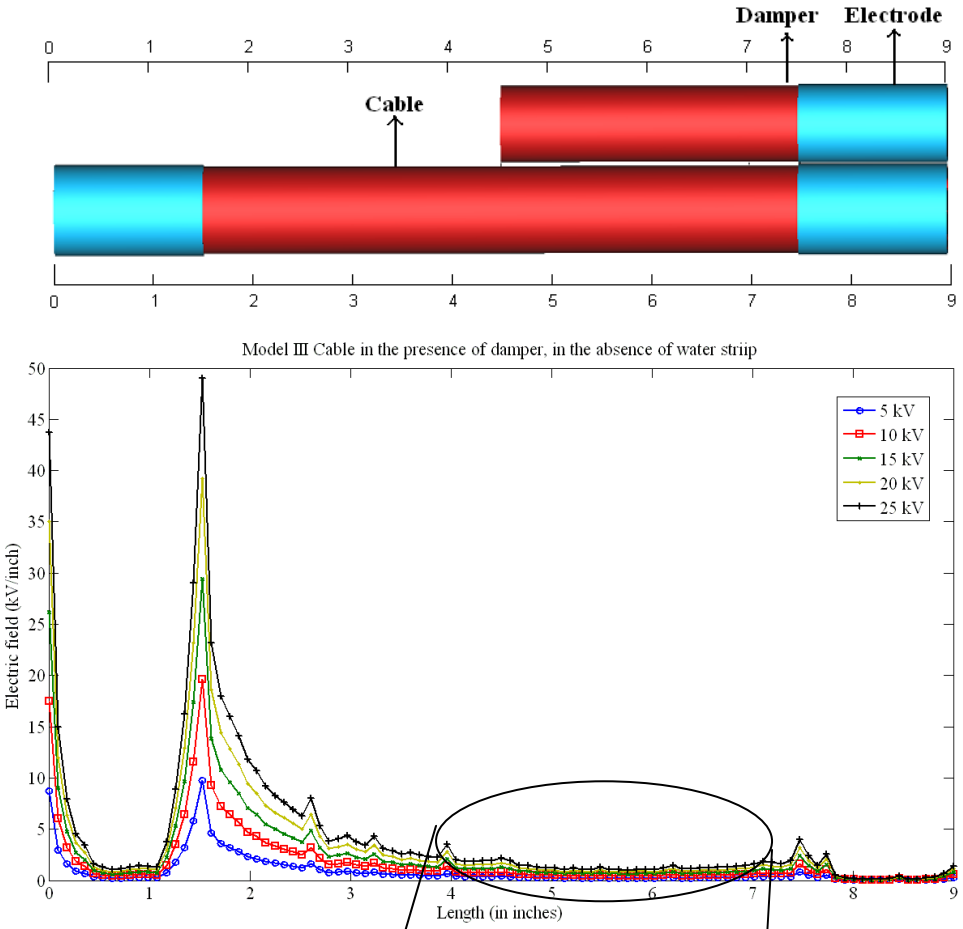

Figure. 55 Electric field on the surface of the cable for model III

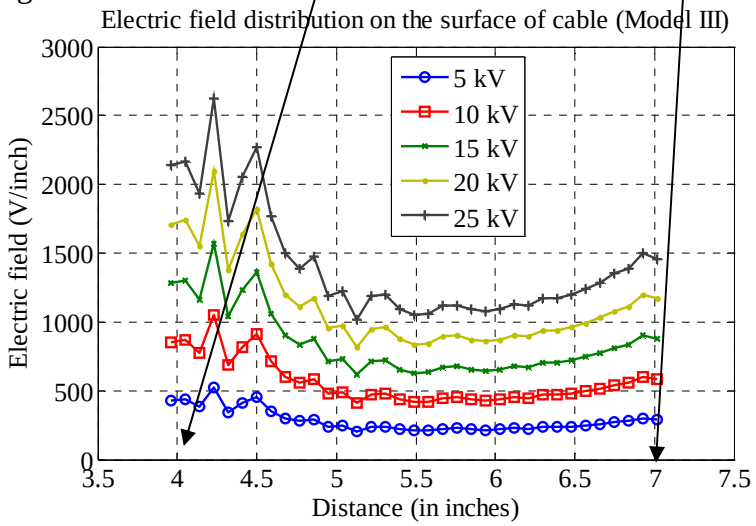

Figure. 56 Electric field for Model III between 4 and 7 inches from high voltage electrode

IV. CABLE MODEL IN THE PRESENCE OF DAMPER AND WATER STRIP

Figure. 57 shows the model used to simulate case IV in COULOMB. A water strip is added to the damper layer. The thickness of the water strip is maintained to be the same. But, the volume occupied by the water strip will be less than the water strip that was placed over the ADSS cable surface in case II. This is due to the fact that the diameter of the damper is lesser than that of the ADSS cable. Figure. 58 show the electric field on the surface of the ADSS cable for case IV. The plot shows that there is an increase in the electric field at the edges of water strip that is at 4.5 inches and at 7 inches from the high voltage electrode end. The maximum when 25 kV was applied to the electrodes is around 10 kV/inch.

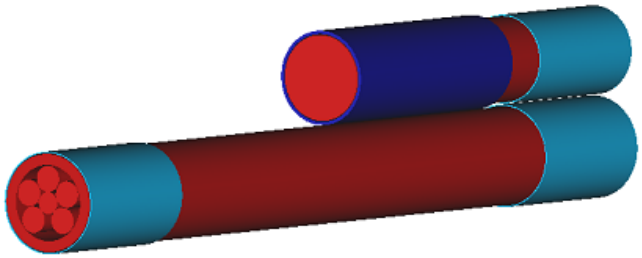

Figure. 57 COULOMB model for case IV

V. SUMMARY OF THE SIMULATIONS

The plots show the effect of damper and the effect of water strip on the electric field distribution on the surface of the cable sample. To stress the effect of water strip over the damper on electric field distribution zoomed in view of the two extreme cases, that is case I and case IV is shown in Figure. 50 and Figure. 59. At 25 kV, the model without damper and water strip had electric field of 1.5 kV/inch. But, the model with both damper and water strip shows that the electric field was around 9.5 kV/inch for an applied voltage of 25 kV. It could be shown

by comparing Figure. 56 with Figure. 59 that it is the presence of water strip on the damper which creates this increase in electric field. The presence of water strip reflects that the surface tends to keep more water on it, which indicates the reduced hydrophobic nature of the surface and indicates that the damper surface is partially wettable. If the surface of the damper is at the same level of hydrophobicity as the ADSS cable, the cable will not damage prematurely. Hampton's criterion states that the arc will extend over the adjacent moisture, if the field exceeds that in the arc [29]. The plots shown above indicate that the electric field distribution on the surface of the cable when the damper installed is five times

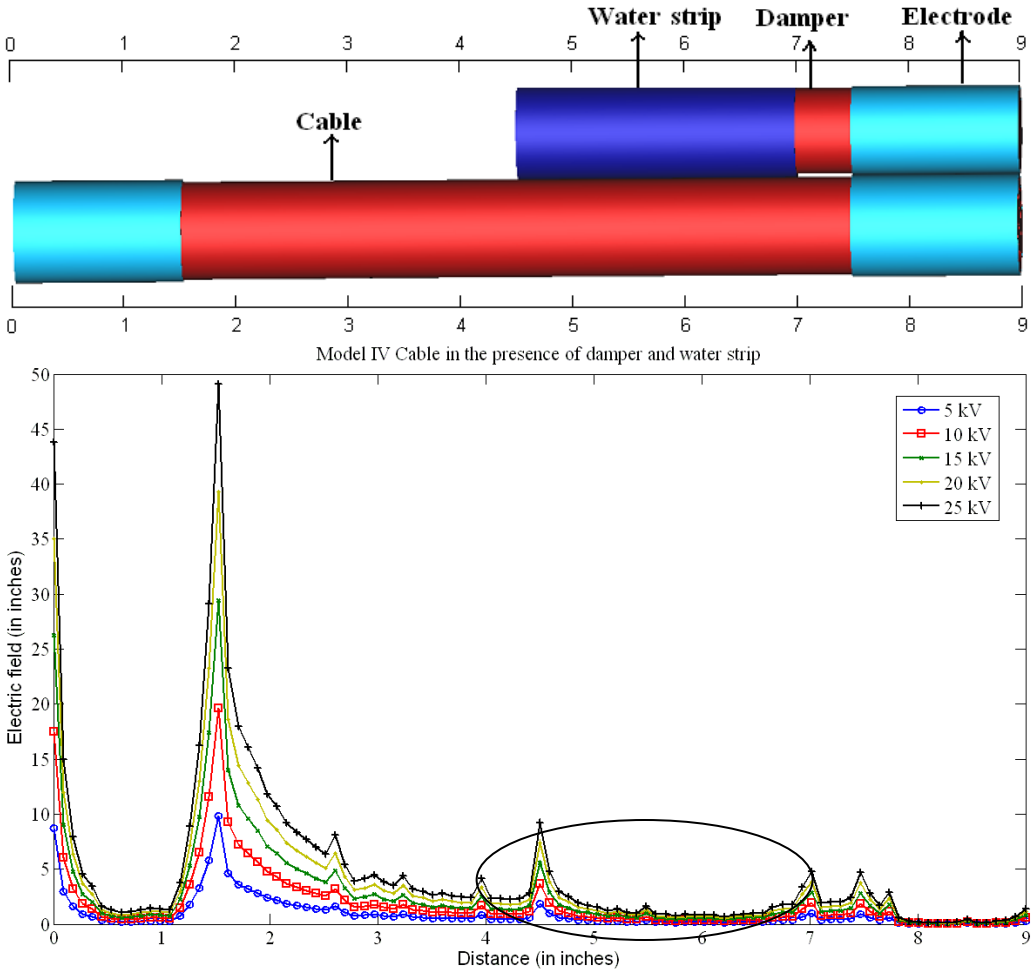

Figure. 58 Electric field on the surface of the cable for model IV

more than a cable without damper. This increase extends the arc from the cable surface to the water droplet in between the damper and cable.

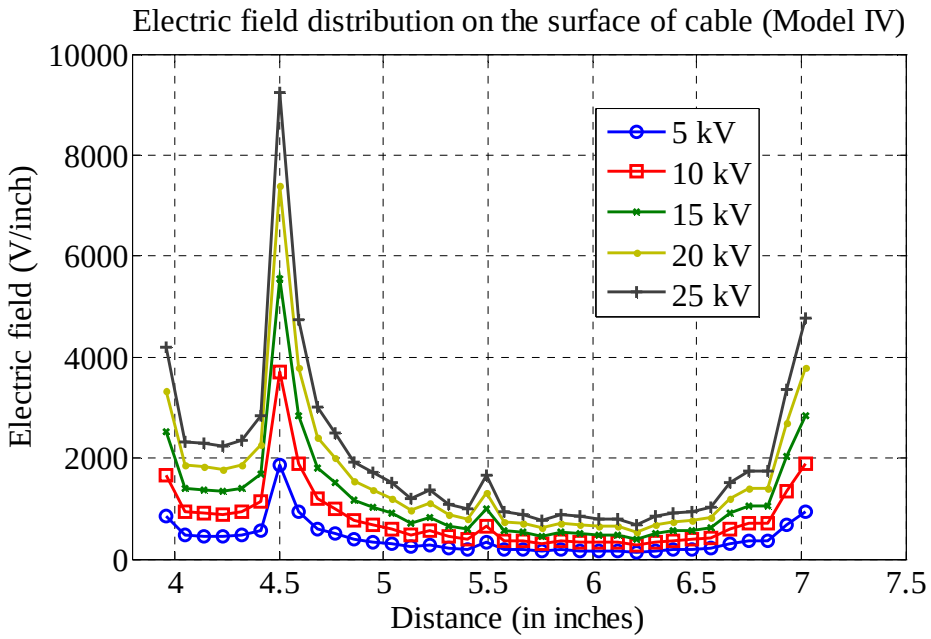

Figure. 59 Electric field for Model IV between 4 and 7 inches from high voltage electrode

Chapter 8

Conclusion and Future work

I. CONCLUSION

A. Ranking ADSS cables using the power needed to damage the dielectric layer

Experiments were conducted on ADSS fiber optic cable samples using two different circuits. The first circuit has a resistor-capacitor bank and the second circuit has only the resistors. These two circuits simulate the pollution existing in the field conditions. The results suggest that the samples tested in the circuit with the RC bank needed more power than the samples that were tested with only a resistor bank.

A novel methodology of classifying the ADSS cable with the power needed to damage the outer dielectric surface of ADSS cable was proposed. Two model systems were presented. Open circuit voltage and short circuit current available in the system for three different pollution levels were calculated. The power available in the system was calculated from the open circuit voltage and short circuit current results.

The experimental results were then used to predict the performance of the cables in the field by analyzing these results with the experimental measurements. For both the models, at the high pollution level, the results suggest that the power was sufficient to deteriorate the cable surface. But, at the low and medium pollution levels, the available power was less than the power needed to deteriorate the cable surface.

B. Effect of damper on dry band arcing:

A novel experimental methodology to test the effect of the damper on dry band arcing was introduced. Samples were tested using this methodology. The results indicate that the cable sample failed earlier at an applied voltage of 15 kV when compared with the sample without a damper over it. Visual observation of the tests discloses that the hydrophobicity of the samples was reduced at the time of failure. This reduction caused water zones to be formed in between the cable and damper surface and formed a conductive path for the leakage current. An increased leakage current flow was observed on the surface of the cable sample with damper over it.

The samples were modeled in commercially available software to observe the electric field distribution. Four models were used for the simulations. The electric field simulations indicate that the electric field was high near the edge of the water strip. In the presence of a water strip, the electric field distribution on the surface increased by a factor of three.

II. CONTRIBUTIONS

i. A new methodology to classify the ranking of ADSS cable using the power needed to deteriorate the outer dielectric cable surface was proposed.

ii. The effect of spiral vibration damper on dry band arcing of ADSS cable was studied.

III. FUTURE WORK

Insulators with semi-conducting layer are gaining interest in the industry. Spiral vibration damper manufacturers have made dampers with such semi-conducting layers on them to avoid dry band arcing between the damper and cables. A study on such a damper could provide interesting results. Not only could the results be useful for the performance of ADSS cables, but also for insulators which uses such a technology.

IV. PUBLICATION

[1] K. Prabakar, G. Karady, “Experimental investigation of dry band arcing on ADSS cables when spiral vibration dampers are installed,” in Electrical insulation conference, Jun. 2011, pp. 226 – 230.

References

[1] H. Murata, *Handbook of optical fibers and cables*. Madison Avenue, New York; 1987, pp. 2-8.

[2] M. Ostendorp, G. Gela, “Fiber optic cables in overhead transmission corridors.” Final report prepared for electric power research institute, Nov 1997, pp. 1-88.

[3] C. N. Carter, “Dry band electrical activity on optical cables separately strung on overhead power lines,” in International wire and cable symposium Proceedings 1988, pp. 117-121.

[4] A. G. W. M. Berkers and J. M. Wetzer, “Electrical stresses on a self-supporting metal-free cable in high voltage networks,” in Fifth international conference on dielectric materials, measurements and applications, 1988, pp. 69-72.

[5] G. Karady, D. Srinivasan, M. Reta-Hernandez, D. Torgerson, M. Tuominen, B. Han, "A mitigation method for dry-band arcing caused deterioration of ADSS fiber optic cables," in IEEE Power Engineering Society Winter Meeting, 2000, pp. 2391-2396.

[6] S. M. Rowland, X. Zhang, K. Kopsidas, "The impact of system voltage on the ageing of all-dielectric self-supporting cables on overhead lines,", in Conference Record of the 2008 IEEE International Symposium on Electrical Insulation, 2008, pp. 641 - 644.

[7] EPRI, “Transmission line reference book: 345kv and above,” Second Edition, Revised, EPRI, 1987, Chapter 3, pp. 63-168.

[8] D. C. Sunkle, J. J. Olenik, M. D. Fullerman, "Determination of damping effectiveness of impact damper on ADSS cable," in International Conference on Transmission and Distribution Construction, Operation and Live-Line Maintenance Proceedings, 2000, pp. 195-201.

[9] PLP (Preformed line products), Application procedure and safety consideration.Available:http://www.preformed.com/preformed/files/AppProc/SP2130-2.pdf.

[10] U. H. P. Oestreich, H. M. Nassar, “Self-supporting dielectric fiber optic cables in high voltage lines,” in International wire and cable symposium Proceedings, 1988, pp. 79-82.

[11] İ. Güneş and Y. Özcelep, “Reliability analysis of ADSS cables using dry band arcing test,” Journal of electrical and electronics engineering-Istanbul univerity, Vol. 8, pp. 593-601, Mar. 2008.

[12] S. Kucuksari, İ. Güneş, G. G. Karady, "A novel method to test the quality of ADSS fiber optic cables installed in transmission lines," in IEEE Bucharest PowerTech, 2009, pp.1-5.

[13] J. D. Shikoski, G. G. Karady, "Analysis of the experimental results for dry band arcing deterioration of adss fiber-optic cables in high electric field," in Power Engineering Society General Meeting, 2007, pp.1-6.

[14] C. N. Carter, "Arc control devices for use on all-dielectric self-supporting, optical cables," in IEE Proceedings on Science, Measurement and Technology, 1993, pp. 357-361.

[15] S. M. Rowland, F. Easthope, "Electrical ageing and testing of dielectric self-supporting cables for overhead power lines," in IEE proceedings on Science, Measurement and Technology, 1993, pp. 351- 356.

[16] G. G. Karady, Y. Lei, D. Srinivasan, M. Tuominen, B. G. Risch, "Experimental investigation of aging effects of dry-band arcing on ADSS fiber-optic cables," in Transmission and Distribution Conference and Exposition, 2003, pp. 898- 903.

[17] S. M. Rowland, Osvaldo de la Cerda, N. R. Haigh, "Implementation of a solution to the problem of dry-band arcing on adss cables," IEEE Transactions on Power Delivery, vol. 22, pp. 703-709, Jan. 2007.

[18] S. M. Rowland, X. Zhang, K. Kopsidas, "Ageing of an ADSS cable sheath on a 132kV overhead transmission line," in Conference on Electrical Insulation and Dielectric Phenomena, 2008, pp. 192-195.

[19] G. G. Karady, S. Devarajan, "Algorithm to predict dry-band arcing in fiber-optic cables," IEEE Transactions on Power Delivery, vol. 16, pp. 286-291, Apr. 2001.

[20] Q. Huang, G. G. Karady, B. Shi, M. Tuorninen, "Calculation of the electric field distribution on ADSS fiber optic cable," in Conference on Electrical Insulation and Dielectric Phenomena, 2003, pp. 379- 382.

[21] S. M. Rowland, K. Kopsidas, I. Cotton, "Modeling of currents on long span, dielectric cables on HV overhead lines," IEEE Transactions on Power Delivery, vol. 22, pp.1138-1144, Apr. 2007.

[22] D. Srinivasan. “Dry-band arcing in arc-dielectric self-supporting fiber-optic cables.” Ph. D. dissertation, Arizona State University, Arizona, 2002.

[23] C. N. Carter, M. A. Waldron, "Mathematical model of dry-band arcing on self-supporting, all-dielectric, optical cables strung on overhead power lines,"

IEE Proceedings on Generation, Transmission and Distribution, vol. 139, pp.185-196, May 1992.

[24] G. G. Karady, S. Devarajan, M. Tuominen, "Novel technique to predict dry-band arcing failure of fiber-optic cables installed on high voltage lines," in International conference on electric power engineering, 1999, pp. 51.

[25] M.W. Tuominen, R. G. Olsen, "Electrical design parameters of all-dielectric-self-supporting fiber optic cable," IEEE Transactions on Power Delivery, vol. 15, no. 3, pp. 940 - 947, Jul 2000.

[26] L. A. Dissado, M. J. Parry, S. V. Wolfe, A. T. Summers, C. N. Cater, " A new sheath evaluation technique for self-supporting optical fiber cables on overhead power lines," in International wire and cable symposium, 1990 pp. 743 – 751.

[27] IEEE, "IEEE Guide for the Application, Maintenance, and Evaluation of Room Temperature Vulcanizing (RTV) Silicone Rubber Coatings for Out-door Ceramic Insulators," *IEEE Std 1523*, 2003.

[28] "IEEE standard for testing and performance for all-dielectric self-supporting fiber optic cable for use on electric utility power lines," IEEE Std 1222-2003.

[29] S. M. Rowland and I. V. Nichols, "Effects of dry-band arc current on ageing of self-supporting dielectric cables in high fields", IEE Proceedings on Science, Measurement and Technology, vol. 143, pp. 10 - 14, 1996.

APPENDIX A

CALCULATION FOR POWER AVAILABLE IN THE SYSTEM

I. INTRODUCTION

This appendix provides the MathCAD® code needed to calculate the power available in the system to create dry band arcing. A model calculation for both the models is presented.

II. MATHCAD® CALCULATIONS

Calculation for Model I

Constants:

$\varepsilon_1 := 8.854187817 \cdot 10^{-12} \cdot \frac{F}{m}$

$N_{sec} := 250$

$a := e^{-i \cdot 120 \cdot deg}$ $mS := 10^{-3} \cdot S$ $\omega := 2 \cdot \pi \cdot 60 \cdot Hz$

$V_{l\_l} := 220kV$ $Span := 500.ft$ $d_{line} := 11.48in$ $d_{cable} := 0.65in$

$R_{layer} := 10^{7} \frac{\Omega}{m}$ $Sag_{line} := 0.02$ $Sag_{cable} := 0.002$

Cable and line co-ordinates:

$x_0 := 0ft$ $y_0 := 21.65m$

$x_1 := -5.3m$ $y_1 := 17.25m$ $x_2 := -4.95m$ $y_2 := 23.85m$ $x_3 := -4.95m$ $y_3 := 30.45m$

$x_4 := 5.3m$ $y_4 := 17.25m$ $x_5 := 4.95m$ $y_5 := 23.85m$ $x_6 := 4.95m$ $y_6 := 30.45m$

$V_{ln} := 1.1 \cdot \frac{V_{l\_l}}{\sqrt{3}}$ $Nu := 0 .. N_{sec} + 1$ $n := 0 .. 6$ $l := 0 .. 6$ $m := 1 .. 6$

Sag of cable and conductors [22]:

$Sag_0 := Span \cdot Sag_{cable}$ $Sag_m := Span \cdot Sag_{line}$

$A_n := y_n - Sag_n$ $b_n := 2 \cdot \frac{\operatorname{acosh}\left(\frac{y_n}{A_n}\right)}{Span}$

$A_n =$

21.345	m
14.202	
20.802	
27.402	
14.202	
20.802	
27.402	

$b_n =$

$2.215 \cdot 10^{-3}$	$\frac{1}{m}$
$8.451 \cdot 10^{-3}$	
$7.02 \cdot 10^{-3}$	
$6.134 \cdot 10^{-3}$	
$8.451 \cdot 10^{-3}$	
$7.02 \cdot 10^{-3}$	
$6.134 \cdot 10^{-3}$	

$Span_1 := \frac{Span}{2}$ $Ya_{n,Nu} := (A_n) \cdot \cosh\left[(b_n) \cdot Span_1 \cdot \left(2 \cdot \frac{Nu}{N_{sec} + 1} - 1\right)\right]$

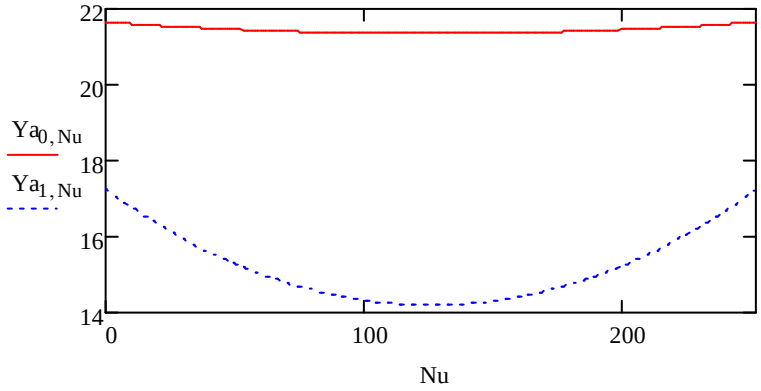

Figure. 60 Sag of transmission line and ADSS cable

$r_0 := \frac{d_{cable}}{2}$ $r_m := \frac{d_{line}}{2}$

Section Capacitances:

$$p(n,l,Nu) := \begin{cases} \dfrac{1}{2\cdot\pi\cdot\varepsilon_1}\cdot\ln\left(\dfrac{Ya_{n,Nu}\cdot 2}{r_n}\right) & \text{if } n = l \\ \dfrac{1}{2\cdot\pi\cdot\varepsilon_1}\cdot\ln\left[\dfrac{\sqrt{\left(x_n - x_l\right)^2 + \left(Ya_{n,Nu} + Ya_{l,Nu}\right)^2}}{\sqrt{\left(x_n - x_l\right)^2 + \left(Ya_{n,Nu} - Ya_{l,Nu}\right)^2}}\right] & \text{otherwise} \end{cases}$$

$$Ps(Nu) := \begin{pmatrix} |p(0,0,Nu)| & |p(0,1,Nu)| & |p(0,2,Nu)| & |p(0,3,Nu)| & |p(0,4,Nu)| & |p(0,5,Nu)| & |p(0,6,Nu)| \\ |p(1,0,Nu)| & |p(1,1,Nu)| & |p(1,2,Nu)| & |p(1,3,Nu)| & |p(1,4,Nu)| & |p(1,5,Nu)| & |p(1,6,Nu)| \\ |p(2,0,Nu)| & |p(2,1,Nu)| & |p(2,2,Nu)| & |p(2,3,Nu)| & |p(2,4,Nu)| & |p(2,5,Nu)| & |p(2,6,Nu)| \\ |p(3,0,Nu)| & |p(3,1,Nu)| & |p(3,2,Nu)| & |p(3,3,Nu)| & |p(3,4,Nu)| & |p(3,5,Nu)| & |p(3,6,Nu)| \\ |p(4,0,Nu)| & |p(4,1,Nu)| & |p(4,2,Nu)| & |p(4,3,Nu)| & |p(4,4,Nu)| & |p(4,5,Nu)| & |p(4,6,Nu)| \\ |p(5,0,Nu)| & |p(5,1,Nu)| & |p(5,2,Nu)| & |p(5,3,Nu)| & |p(5,4,Nu)| & |p(5,5,Nu)| & |p(5,6,Nu)| \\ |p(6,0,Nu)| & |p(6,1,Nu)| & |p(6,2,Nu)| & |p(6,3,Nu)| & |p(6,4,Nu)| & |p(6,5,Nu)| & |p(6,6,Nu)| \end{pmatrix}$$

$$Cs(Nu) := Ps(Nu)^{-1}$$

$$Ca_{Nu} := \frac{Span}{N_{sec} + 1}\cdot\left|Cs(Nu)_{0,1}\right| \qquad Ca_0 = 7.025\times 10^{-13}\,F$$

$$Ca_{N_{sec}+1} = 7.025\times 10^{-13}\,F$$

$$Ca1_{Nu} := \frac{Span}{N_{sec} + 1}\cdot\left|Cs(Nu)_{0,4}\right| \qquad Ca1_0 = 7.025\times 10^{-13}\,F$$

$$Ca1_{N_{sec}+1} = 7.025\times 10^{-13}\,F$$

$$Cb_{Nu} := \frac{Span}{N_{sec} + 1}\cdot\left|Cs(Nu)_{0,2}\right| \qquad Cb_0 = 9.191\times 10^{-13}\,F$$

$$Cb_{N_{sec}+1} = 9.191\times 10^{-13}\,F$$

$$Cb1_{Nu} := \frac{Span}{N_{sec} + 1} \cdot \left| Cs(Nu)_{0,5} \right| \qquad Cb1_0 = 9.191 \times 10^{-13}\,F \qquad Cb1_{N_{sec}+1} = 9.191 \times 10^{-13}\,F$$

$$Cc_{Nu} := \frac{Span}{N_{sec} + 1} \cdot \left| Cs(Nu)_{0,3} \right| \qquad Cc_0 = 3.748 \times 10^{-13}\,F \qquad Cc_{N_{sec}+1} = 3.748 \times 10^{-13}\,F$$

$$Cc1_{Nu} := \frac{Span}{N_{sec} + 1} \cdot \left| Cs(Nu)_{0,6} \right| \qquad Cc1_0 = 3.748 \times 10^{-13}\,F \qquad Cc_{N_{sec}+1} = 3.748 \times 10^{-13}\,F$$

$$Cg_{Nu} := \frac{Span}{N_{sec} + 1} \cdot \sum_{k=0}^{6} Cs(Nu)_{0,k} \qquad Cg_0 = 8.385 \times 10^{-13}\,F \qquad Cg_{N_{sec}+1} = 8.385 \times 10^{-13}\,F$$

$$Cth_{Nu} := Ca_{Nu} + Cb_{Nu} + Cc_{Nu} + Ca1_{Nu} + Cb1_{Nu} + Cc1_{Nu} + Cg_{Nu}$$

$$Cth_0 = 4.831 \times 10^{-12}\,F \qquad Cth_{N_{sec}+1} = 4.831 \times 10^{-12}\,F$$

$$Rc_{Nu} := \frac{Span}{N_{sec} + 1} \cdot R_{layer}$$

$$Vs_{Nu} := V_{ln} \cdot \frac{\left(Ca_{Nu} + a^2 Cb_{Nu} + a\,Cc_{Nu} + Ca1_{Nu} + a^2 Cb1_{Nu} + a\,Cc1_{Nu} \right)}{Cth_{Nu}}$$

$$n := 1 .. N_{sec}$$

$$X_{Nu} := \frac{1}{j \cdot \omega \cdot Cth_{Nu}} \qquad Yx_{Nu} := \frac{1}{X_{Nu}} \qquad Yra := \frac{1}{Rc_0}$$

Voltage and current distribution

$$temp_n := \frac{Yx_n}{Yx_n + 2\cdot Yra} \qquad tempo_n := \frac{Yra}{Yx_n + 2\cdot Yra}$$

$$Varib_n := \begin{cases} tempo_n & \text{if } n = 1 \\ \dfrac{tempo_n}{1 - Varib_{n-1}\cdot tempo_n} & \text{otherwise} \end{cases}$$

$$Varia_n := \begin{cases} Vs_n\cdot temp_n & \text{if } n = 1 \\ \left(\dfrac{Vs_n\cdot temp_n + Varia_{n-1}\cdot tempo_n}{1 - Varib_{n-1}\cdot tempo_n}\right) & \text{otherwise} \end{cases}$$

$n := N_{sec} .. 1$

$$Vr_n := \begin{cases} Varia_n & \text{if } n = N_{sec} \\ \left(Varia_n + Vr_{n+1}\cdot Varib_n\right) & \text{otherwise} \end{cases}$$

$Vr_0 := 0 \qquad Vr_{N_{sec}+1} := 0$

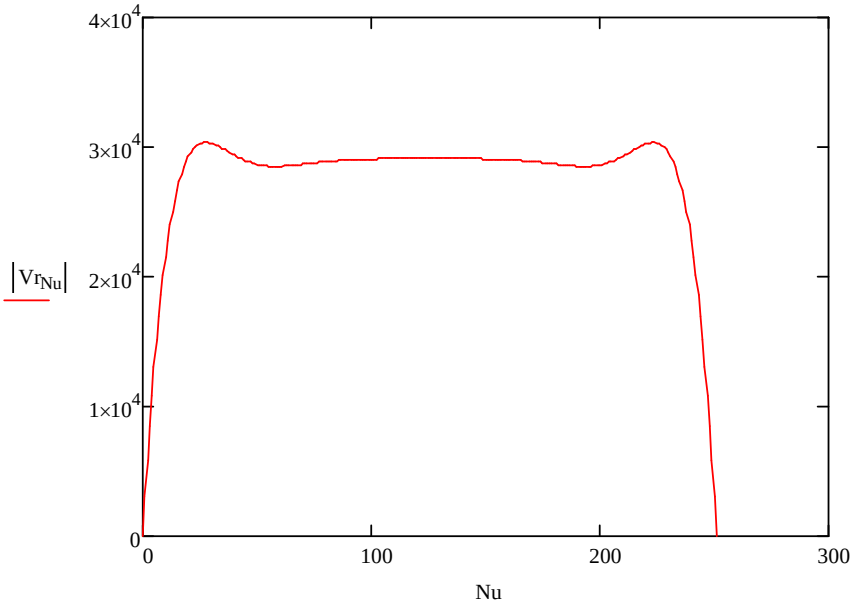

Figure. 61Voltage distribution on the surface of ADSS cable

$N2 := 0.. N_{sec} \qquad i_{sur_{N2}} := \left(Vr_{N2+1} - Vr_{N2}\right)\cdot Yra$

$$Ythev := \left| \begin{array}{l} Ys_{N_{sec}} \leftarrow \dfrac{Yra \cdot Yx_{N_{sec}}}{Yra + Yx_{N_{sec}}} \\ \text{for } k \in N_{sec} - 1 .. 1 \\ \quad \left| \begin{array}{l} Yp_k \leftarrow Yx_k + Ys_k \\ Ys_{k-1} \leftarrow \dfrac{Yra \cdot Yp_k}{Yra + Yp_k} \end{array} \right. \\ Ys_0 \end{array} \right. \qquad Zthev := \frac{1}{Ythev}$$

Open circuit voltage and short circuit current

$$Isc := \left(i_{sur_0}\right) \qquad Voc := Isc \cdot Zthev \qquad Power := Voc \cdot Isc$$

$$\left|Re(Power)\right| = 10.944W$$

Calculation for model II:

$$V_{LL} := 220kV \qquad \varepsilon_o := \frac{10^{-9}}{36 \cdot \pi} \cdot \frac{F}{m} \qquad a := e^{-j \cdot 120deg} \qquad \omega := 2 \cdot \pi \cdot 60Hz$$

$$Span := 500ft = 152.4m \qquad d_{line} := 11.48in \qquad d_{ADSS} := 0.65in \qquad R_{ADSS} := 10^5 \cdot \frac{\Omega}{m}$$

$$Sag_{line} := 2\% \qquad Sag_{ADSS} := 0.2\% \qquad N_{sec} := 250$$

Cable and line co-ordinates

$$x := \begin{pmatrix} 0m \\ -11.88m \\ 0m \\ 11.88m \end{pmatrix} \qquad y := \begin{pmatrix} 30.48m \\ 37.18m \\ 37.18m \\ 37.18m \end{pmatrix} \qquad V_{ln} := 1.1 \cdot \frac{V_{LL}}{\sqrt{3}} = 139.719 \cdot kV$$

$$N := 0 .. N_{sec} + 1 \qquad n := 0 .. 3 \qquad l := 0 .. 3$$

Sag of cable and conductors [22]

$$Sag_n := Span \cdot if\left(n = 0, Sag_{ADSS}, Sag_{line}\right) \qquad A_n := y_n - Sag_n \qquad b_n := \frac{2}{Span} \cdot acosh\left(\frac{y_n}{A_n}\right)$$

$$Ya_{n,N} := A_n \cdot \cosh\left[b_n \cdot \frac{Span}{2} \cdot \left(\frac{2 \cdot N}{N_{sec} + 1} - 1\right)\right]$$

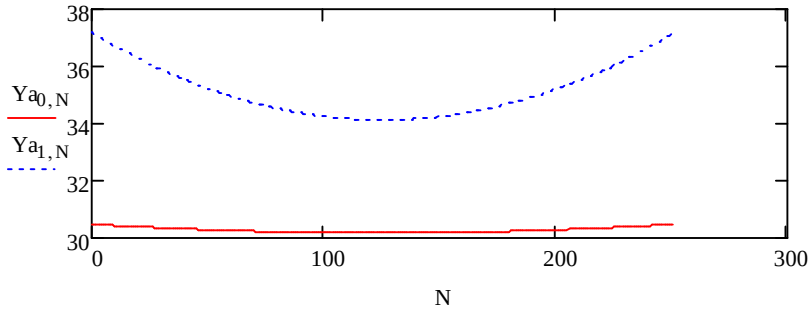

Figure. 62 Sag of transmission line and ADSS cable

$$r_n := \text{if}\left(n = 0, \frac{d_{ADSS}}{2}, \frac{d_{line}}{2}\right)$$

$$p(n,l,N) := \text{if}\left[n = l, \frac{1}{2\cdot\pi\cdot\varepsilon_o}\cdot\ln\left(\frac{2\cdot Ya_{n,N}}{r_n}\right), \frac{1}{2\cdot\pi\cdot\varepsilon_o}\cdot\ln\left[\frac{\sqrt{(x_n - x_l)^2 + (Ya_{n,N} + Ya_{l,N})^2}}{\sqrt{(x_n - x_l)^2 + (Ya_{n,N} - Ya_{l,N})^2}}\right]\right]$$

$$Ps(N) := \begin{pmatrix} p(0,0,N) & p(0,1,N) & p(0,2,N) & p(0,3,N) \\ p(1,0,N) & p(1,1,N) & p(1,2,N) & p(1,3,N) \\ p(2,0,N) & p(2,1,N) & p(2,2,N) & p(2,3,N) \\ p(3,0,N) & p(3,1,N) & p(3,2,N) & p(3,3,N) \end{pmatrix}$$

Section Capacitances

$$Cs(N) := Ps(N)^{-1}$$

$$Ca_N := \frac{Span}{N_{sec}+1}\cdot\left|Cs(N)_{0,1}\right| \qquad Ca_0 = 0.639\cdot pF \qquad Ca_{N_{sec}+1} = 0.639\cdot pF$$

$$Cb_N := \frac{Span}{N_{sec}+1}\cdot\left|Cs(N)_{0,2}\right| \qquad Cb_0 = 1.231\cdot pF \qquad Cb_{N_{sec}+1} = 1.231\cdot pF$$

$$Cc_N := \frac{Span}{N_{sec}+1}\cdot\left|Cs(N)_{0,3}\right| \qquad Cc_0 = 0.639\cdot pF \qquad Cc_{N_{sec}+1} = 0.639\cdot pF$$

$$Cg_N := \frac{Span}{N_{sec}+1}\cdot\sum_{k=0}^{3} Cs(N)_{0,k} \qquad Cg_0 = 1.83\cdot pF \qquad Cg_{N_{sec}+1} = 1.83\cdot pF$$

$$Ra := \frac{Span}{N_{sec}+1}\cdot R_{ADSS} \qquad Ra = 6.072\times 10^4\cdot\Omega$$

$$C_{th_N} := Cg_N + Ca_N + Cb_N + Cc_N \qquad X_N := \frac{1}{j \cdot \omega \cdot C_{th_N}}$$

$$Xa_N := \frac{1}{j \cdot \omega \cdot Ca_N} \qquad Xb_N := \frac{1}{j \cdot \omega \cdot Cb_N} \qquad Xc_N := \frac{1}{j \cdot \omega \cdot Cc_N} \qquad Xg_N := \frac{1}{j \cdot \omega \cdot Cg_N}$$

$$Vs_N := V_{ln} \cdot \frac{\left(\frac{1}{Xa_N} + \frac{a^2}{Xb_N} + \frac{a}{Xc_N} \right)}{\left(\frac{1}{Xa_N} + \frac{1}{Xb_N} + \frac{1}{Xc_N} + \frac{1}{Xg_N} \right)}$$

$$Yra := \frac{1}{Ra} \qquad Yx_N := \frac{1}{X_N}$$

Voltage and current distribution

$$n := 1.. \left(N_{sec}\right)$$

$$temp_n := \frac{Yx_n}{Yx_n + 2 \cdot Yra} \qquad tempo_n := \frac{Yra}{Yx_n + 2 \cdot Yra}$$

$$Varib_n := \begin{cases} tempo_n & \text{if } n = 1 \\ \dfrac{tempo_n}{1 - Varib_{n-1} \cdot tempo_n} & \text{otherwise} \end{cases}$$

$$Varia_n := \begin{cases} Vs_n \cdot temp_n & \text{if } n = 1 \\ \left(\dfrac{Vs_n \cdot temp_n + Varia_{n-1} \cdot tempo_n}{1 - Varib_{n-1} \cdot tempo_n} \right) & \text{otherwise} \end{cases}$$

$$n := N_{sec}.. 1$$

$$Vr_n := \begin{cases} Varia_n & \text{if } n = N_{sec} \\ \left(Varia_n + Vr_{n+1} \cdot Varib_n\right) & \text{otherwise} \end{cases}$$

$$Vr_0 := 0 \qquad Vr_{N_{sec}+1} := 0$$

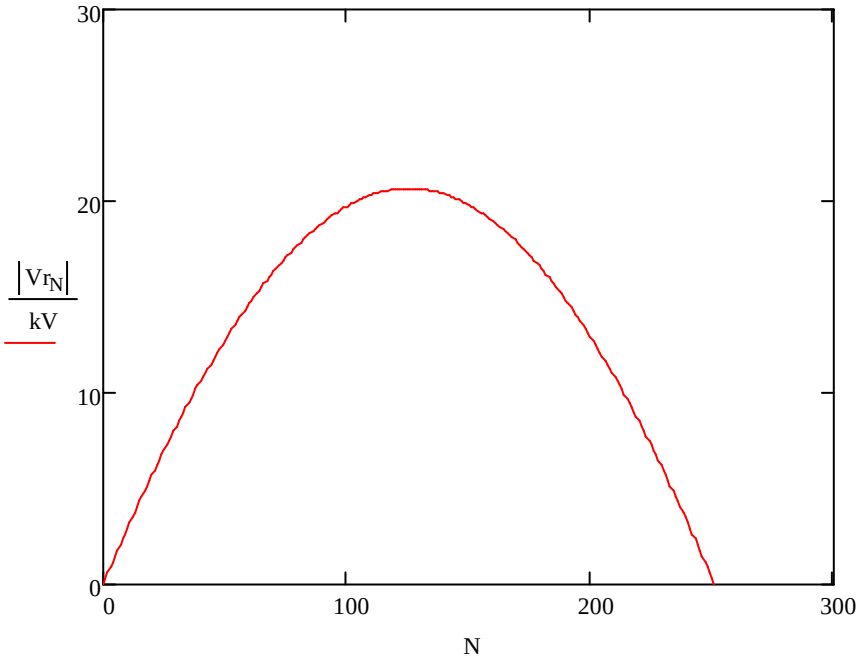

Figure. 63 Voltage distribution

$N2 := 0 .. N_{sec}$

$i_{sur_{N2}} := \left(Vr_{N2+1} - Vr_{N2}\right) \cdot Yra$

$i_{sur_0} = \left(-4.959 \times 10^{-3} - 7.55i \times 10^{-5}\right) A$

Open circuit voltage and short circuit current

$$Isc := \left(i_{sur_0}\right)$$

$$Ythev := \left| \begin{array}{l} Ys_{N_{sec}} \leftarrow \dfrac{Yra \cdot Yx_{N_{sec}}}{Yra + Yx_{N_{sec}}} \\ \text{for } k \in N_{sec} - 1 .. 1 \\ \quad \left| \begin{array}{l} Yp_k \leftarrow Yx_k + Ys_k \\ Ys_{k-1} \leftarrow \dfrac{Yra \cdot Yp_k}{Yra + Yp_k} \end{array} \right. \\ Ys_0 \end{array} \right.$$

$$Zthev := \frac{1}{Ythev}$$

$$Voc := Isc \cdot Zthev$$

$$Power := Voc \cdot Isc$$

$$\left|Re(Power)\right| = 105.837 \cdot W$$

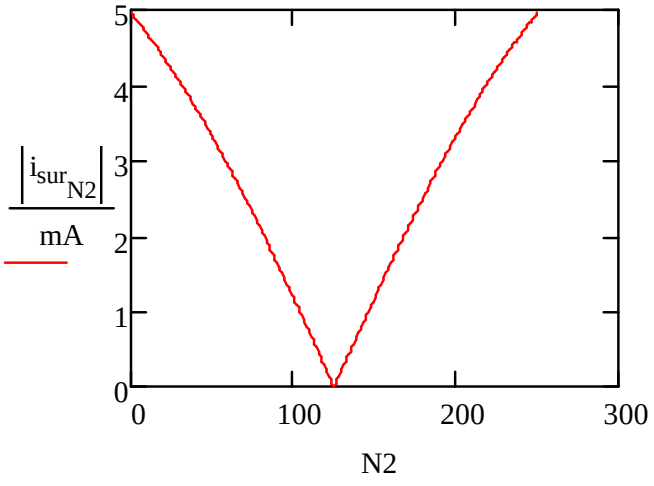

Figure. 64 Current distribution